

An Illustration of Modeling Cataclysmic Variables: HST, FUSE, SDSS Spectra of SDSSJ080908.39+381406.2¹

Albert P. Linnell², D.W.Hoard³, Paula Szkody⁴, Knox S. Long⁵, Ivan Hubeny⁶, Boris Gänsicke⁷, and Edward M.Sion⁸

²*Department of Astronomy, University of Washington, Box 351580, Seattle, WA 98195-1580*

³*Spitzer Science Center, California Institute of Technology, Mail Code 220-6, 1200 E. California Blvd., Pasadena, CA 91125*

⁴*Department of Astronomy, University of Washington, Box 351580, Seattle, WA 98195-1580*

⁵*Space Telescope Science Institute, 3700 San Martin Drive, Baltimore, MD 21218*

⁶*Steward Observatory and Department of Astronomy, University of Arizona, Tucson, AZ 85721*

⁷*Department of Physics, University of Warwick, CV4 7AL, Coventry, UK*

⁸*Department of Astronomy and Astrophysics, Villanova University, Villanova, PA 19085*

²linnell@astro.washington.edu

³hoard@ipac.caltech.edu

⁴szkody@astro.washington.edu

⁵long@stsci.edu

⁶hubeny@as.arizona.edu

⁷boris.gaensicke@warwick.ac.uk

⁸edward.sion@villanova.edu

ABSTRACT

FUSE, *HST* and SDSS spectra of the cataclysmic variable SDSSJ080908.39+381406.2 provide a spectral flux distribution from 900–9200Å. This data set is used to illustrate procedures for calculating and testing system models. The spectra are not contemporaneous. The illustrations are based on a system with a $1.0M_{\odot}$ white dwarf, a $0.30M_{\odot}$, 3500K, Roche lobe-filling secondary star, and

¹Based on observations made with the NASA/ESA Hubble Space Telescope, obtained at the Space Telescope Science Institute, which is operated by the Association of Universities for Research in Astronomy, Inc. under NASA contract NAS5-26555, the NASA-CNES-CSA *Far Ultraviolet Explorer*, which is operated for NASA by the Johns Hopkins University under NASA contract NAS5-32985, and with the Apache Point Observatory 3.5 m telescope, which is operated by the Astrophysical Research Corporation.

an accretion disk extending to the tidal cutoff radius. Assuming a similar accretion state for the non-simultaneous spectra, the best standard model fit is with a mass transfer rate of $3.0 \times 10^{-9} M_{\odot} \text{yr}^{-1}$. Extensive simulations demonstrate that the accretion disk must be truncated at its inner edge if the temperature profile follows the standard model, but truncated models face severe objections, which we address. Following additional simulation tests, we obtain a model accretion disk with a temperature profile comparable to the profile for SW Sex as determined from tomographic image reconstruction. This model fits the discovery SDSS spectrum well but has a flux deficit in the UV and FUV. Emission from a white dwarf is a plausible source of additional flux. Adding this source to the disk synthetic spectrum produces FUV flux that can explain the observed flux.

An additional (archival) SDSS spectrum is fainter by about 0.3 magnitude in the optical. Additional analysis showed that UV residuals from a model fitting the archival optical wavelength spectrum are unacceptably large. Contemporaneous spectra from all wavelength regions would be necessary for a reliable system model. Our discussion illustrates how this conclusion follows from the system models.

Subject headings: accretion, accretion disks — novae, cataclysmic variables — stars: individual(SDSSJ0809) — ultraviolet: stars — white dwarfs

1. Introduction

Cataclysmic variables (CVs) are semi-detached binary stars in which a late main sequence star loses mass onto a white dwarf (WD) via Roche lobe overflow. In systems containing a non-magnetic WD, accretion proceeds through a viscous disk. However, in systems containing a magnetic WD, accretion may proceed directly from the inner Lagrangian point onto field lines in the strong field case, or through a partial disk in the case of intermediate field strength. The group of CVs that have typical orbital periods between 3-4 hrs, strong single-peaked Balmer emission, strong HeII emission and deep central absorption in the Balmer and HeI lines (usually near orbital phase 0.5) are called the SW Sex stars (e.g., Honeycutt, Schlegel, & Kaitchuck (1986); Szkody & Piché (1990); Thorstensen et al. (1991)). As a group, their orbital periods place the SW Sex stars at the top of the period gap, which likely is an aspect of the normal secular evolution of the CV population (Warner 1995). The SW Sex stars typically have high mass accretion rates and a few of them may have intermediate strength magnetic fields as evinced from weak polarization (Rodriguez-Gil et al. 2001). See Warner (1995) for a thorough review of CV types and behaviors.

The observational data that are commonly available to study CVs include spectra and photometry. Deduction of the physical properties of these binary stars depends on simulation of the observations, based on a physical model believed to represent reality with adequate accuracy. The accretion disk is typically the most important radiating component in a CV over a wide range of wavelengths. A common practice has been to use synthetic stellar spectra to simulate the accretion disk (la Dous (1987, 1994)). More recently, Wade & Hubeny (1998) have calculated a set of models based on the TLUSTY program. It is desirable to have a simulation program that calculates an accretion disk *ab initio*, given an orbital inclination, WD mass, and mass transfer rate. A combination of the programs TLUSTY (Hubeny 1988) and BINSYN (Linnell & Hubeny 1996) provides this feature. The details of how the calculation takes place, in the context of a specific system, have not been described in the literature. The availability of both *HST* and *FUSE* data combined with a good SDSS spectrum of a bright system (few systems provide this combination) provides the impetus for modeling this system. Since the data were not contemporaneous, a definitive solution is not available. However, as we show later, we are able to find a solution which satisfactorily represents the data set. At the same time, the data set provides a very useful basis to illustrate the details of building and testing system models, and the results turn out to be of considerable intrinsic interest.

2. The SDSSJ0809 system

The Sloan Digital Sky Survey (York et al. 2000) provides 5 color photometry (ugriz) and spectra (3800-9200Å at a resolution of 3Å) of the survey objects. The survey has identified a large number of CV systems (Szkody et al. 2002, 2003, 2004, 2005).

During the survey, SDSS J080908.39+381406.2 (hereafter abbreviated as SDSSJ0809) was discovered as a bright CV ($g \sim 15.6$) (Szkody et al. 2003). The discovery paper provides the photometric colors and optical spectrum of SDSSJ0809 as well as the results of time-resolved followup spectra obtained over the course of 3 hrs. The SDSS spectrum shows a steep blue continuum with strong Balmer emission lines as well as prominent emission from He II $\lambda 4686$ and the CN blend at 4640Å. The time-resolved spectra show deep and transient absorption in the Balmer and HeI lines. If the $H\alpha$ and $H\beta$ radial velocities indicate orbital phases, then the deep absorptions occur near orbital phase 0.5 (Szkody et al. 2003), which is a hallmark of the SW Sex stars. However, we lack any confirming evidence (eclipses) and we are presently unable to make any definite statement about orbital phases. There was no noticeable eclipse during the 3 hrs of observations and the radial velocity curve constructed from the $H\alpha$ and $H\beta$ emission lines indicated an orbital period near 2.4 hrs. However, the

shortness of the data interval precluded the determination of an accurate period. Recent photometry over many nights indicates that the period is 192 min (more typical for SW Sex stars) and there may be a shallow or partial eclipse (Rodriguez-Gill et al., in preparation) with amplitude of less than about 0.1 magnitude. We will use the 192 min period throughout this paper.

Due to the brightness of this system, ultraviolet measurements were possible with both the Far Ultraviolet Spectroscopic Explorer (*FUSE*) and the Hubble Space Telescope (*HST*) and were used to explore the accretion parameters and geometry of the high accretion regime. In the high inclination SW Sex star DW UMa, which shows deep eclipses, the accretion disk completely obscures the WD and inner disk during high states of accretion (Knigge et al. 2004). When the accretion is reduced during low states of mass transfer, the underlying WD is revealed and it is very hot (near 50,000K (Araujo-Betancor et al. 2003)). Most SW Sex stars have high inclinations and deep eclipses such that, as in DW UMa, the WD is hidden from view by the accretion disk. We observed SDSSJ0809 in the hope that its apparent lower inclination (as evinced by the lack of deep eclipses) might permit a more direct view of the WD and inner disk, and thus allow us to explore the characteristics of these components of an SW Sex star. An objective of this investigation is to determine the extent to which the large SDSS spectral range, combined with spectra from *HST* and *FUSE*, together with related collateral information, permit development of a self-consistent model.

As the following sections indicate, we have a single *HST* spectrum, and two sets of SDSS and *FUSE* observations. None of the observations are simultaneous. The photometric observations Rodriguez-Gill et al. were obtained some 300 days after the *HST* exposure and continued over an interval of 26 days. The photometry shows only minor orbital variation, with an amplitude of 0.1 magnitude that may indicate a grazing eclipse, but with no systematic trend. There is consistent overlap of the *HST* and one of the *FUSE* observations. Since the SDSS photometry, the first SDSS spectrum, the subsequent APO spectroscopy, the Rodriguez-Gil photometry and the optical measurement from the *HST* snapshot all agree (to ± 0.1 mag), we first treated the system as if it is constant at all observed wavelengths longward of the *FUSE* observations.

3. *FUSE* Observations and Data Processing

We observed SDSSJ0809 with *FUSE* during two time intervals approximately 1 year apart; Observation 1 occurred on 28 Mar 2003 and Observation 2 occurred on 16–17 Mar 2004. Because of the *FUSE* orbital constraints, each observation was divided into several exposures (4 exposures for Observation 1, 8 exposures for Observation 2) – see Table 1 for

the *FUSE* observing log. All data were obtained using the LWRS aperture and TTAG accumulation mode (for *FUSE* spacecraft and instrument details see, for example, Sahnou et al. 2000¹). We used the CalFuse v3.0.7 pipeline software to prepare intermediate data files from the raw data files obtained during each *FUSE* exposure. We then used the IDL routine `cf_edit` v2.9², as well as custom-built IDL routines, to extract spectra from the various detector and mirror segments and combine them into a time-averaged spectrum for each observation. The time-averaged spectra have total equivalent exposure times of ≈ 8.4 ksec for Observation 1 and ≈ 10 ksec for Observation 2 (total exposure times from the mirror/detector pairs differ by up to $\sim 5\%$ due to differences in rejected data; the combined spectrum accounts for this by weighting by exposure time when combining data from different mirror/detector pairs). The final combined spectra (see Figures 1 and 2) were rebinned onto a uniform wavelength scale with dispersion $0.20 \text{ \AA pixel}^{-1}$ by averaging flux points from the original dispersion ($0.013 \text{ \AA pixel}^{-1}$) into wavelength bins of width 0.20 \AA .

4. Analysis of FUV Spectra

Our initial plan was to combine the two *FUSE* data sets to improve the S/N of the final time-averaged spectrum. However, it was apparent that the spectra obtained from the two observations were somewhat different, so we treated them separately. Shortward of $\approx 1000 \text{ \AA}$ the two spectra are approximately equivalent, although this apparent agreement is likely due mainly to the weak detection at these short wavelengths. None of the sulfur or silicon emission lines often seen in FUV spectra of CVs in this wavelength region (e.g., Hoard et al. 2003; Froning et al. 2001; Long et al. 1994) are detected in SDSSJ0809 (see the top panels of Figures 1 and 2). The C III, N III emission complex is possibly present in both spectra; however, it coincides with the wavelengths of a series of airglow features, which makes a definitive detection difficult.

At longer wavelengths, the Observation 2 spectrum is approximately twice as bright in the continuum as the Observation 1 spectrum; for example, the “mean” continuum level at 1155 \AA is $\approx 0.75 \times 10^{-14} \text{ erg s}^{-1} \text{ cm}^{-2} \text{ \AA}^{-1}$ in the Observation 1 spectrum and $\approx 1.5 \times 10^{-14} \text{ erg s}^{-1} \text{ cm}^{-2} \text{ \AA}^{-1}$ in the Observation 2 spectrum.

There are also differences in the ionic features present at $\lambda > 1000 \text{ \AA}$ in each spectrum. In the Observation 1 spectrum, the S+Si line complexes at $1055\text{--}1085 \text{ \AA}$ and $1105\text{--}1130 \text{ \AA}$ are

¹Also see the *FUSE* Science Center web page at <http://fuse.pha.jhu.edu/>.

²Written by Don Lindler and available at http://fuse.pha.jhu.edu/analysis/fuse_idl_tools.html.

present as broad, undifferentiated “humps” in the continuum. However, in the Observation 2 spectrum, these same wavelength regions contain clearly differentiated emission and/or absorption features. The most striking difference is in the C+N+O line complex at 1165–1185Å. In the Observation 1 spectrum, this is present mainly as a fairly strong emission feature (strongest of the non-airglow lines) at the wavelengths spanned by the O III multiplet. In the Observation 2 spectrum, on the other hand, this line complex displays a profile consisting of a broad hump from 1165–1185Å, with a possible discrete O III emission component, and deep absorption (reaching down to at least the level of the underlying continuum) at the wavelengths spanned by the C III+N I multiplets.

The O VI lines at $\lambda\lambda 1031.9, 1037.6\text{\AA}$, which are often among the most prominent emission features in the FUV spectra of CVs with ongoing accretion (e.g., Hoard et al. 2005, 2003, 2002; Mauche 1999), are only weakly present in both spectra of SDSSJ0809. In addition, the line profiles of O VI appear to be in emission on the blue side and absorbed on the red side (similar to the shape of the C+N+O line complex at 1165–1185Å in Observation 2). Detection of the S III multiplet at 1012–1021Å is even weaker (or non-existent) compared to O VI in both spectra. Neither spectrum displays detectable Si III features at 1144Å.

The total exposure time for each of the time-averaged FUV spectra of SDSSJ0809 is shorter than the orbital period of the CV (75–85% of $P_{\text{orb}} = 192$ min). However, the total orbital phase coverage during a given observation differs from the other observation by only about 10% and spans most of an orbit. Thus, we believe that the differences between the spectra are not likely to be due only to differences in lines-of-sight through the orbital geometry. In any case, the current estimate of the orbital period of SDSSJ0809 is not known precisely enough to preserve cycle count well enough from Observation 1 to Observation 2 that we could compare relative phases of the two *FUSE* spectra.

The Observation 1 spectrum, which we designate as *FUSE1*, accords with the HST spectrum in the wavelength overlap region better than the Observation 2 spectrum. The Observation 2 spectrum difference from the Observation 1 spectrum could arise from a change in the accretion disk (discussed subsequently) in the time interval between the two observations.

5. *HST* Observations

SDSSJ0809 was observed on 2004 Apr 29 as part of an *HST* Space Telescope Imaging Spectrograph (STIS) snapshot program (see Gänsicke et al. (2003) for a description of this program). Using the STIS/CCD acquisition image, we determined that the magnitude in

the F28x50LP filter ($\sim 5500 - 11,000\text{\AA}$) was about 15.5. The STIS spectrum is an 800-sec exposure obtained with the G140L grating, in accum mode, which provided wavelength coverage from 1100–1700 \AA with a resolution of 1.2 \AA . The data were reduced with CALSTIS (V2.13b) which corrected for the decaying sensitivity of the grating.

The spectrum is shown in Figure 3. The continuum displays a downturn near $\text{Ly}\alpha$ and weak emission lines of CIII, NV, CII, SiIV and CIV can be identified. The lines are noticeably weaker than those in the high state STIS spectrum of DW UMa (Knigge et al. 2004), consistent with a lower inclination for SDSSJ0809. The absorption cores at the SiIV doublet wavelengths, superposed on the overlapping doublet emission, and the doubled appearance of the CIV lines are similar to the STIS spectrum of DW UMa at phase 0.5 (Knigge et al. 2004), when the absorption events characteristic of SW Sex stars are most prominent. A number of additional line identifications in Figure 3 mark absorption cores associated with broad emission features; in most cases the absorption core goes below the continuum level, indicating a substantial column density along the line of sight. Unfortunately, we cannot determine the phase of the SDSSJ0809 STIS spectrum as there currently is no orbital ephemeris.

6. SDSS and APO Observations

The discovery spectrum of SDSS0809 from MJD52251 is described in Szkody et al. (2003) and is reproduced here in Figure 4. The exposure time, 5803 sec, spans approximately half an orbital cycle. There is no indication of a Balmer discontinuity. The SDSS photometry for SDSSJ0809 gave $g=15.61$, and the 5500 \AA flux in the SDSS spectrum gave an approximate V magnitude of ~ 15.4 .

The Apache Point Observatory (APO) follow-up spectra, obtained over 2.9 hours, provided a radial velocity curve in both $\text{H}\alpha$ and $\text{H}\beta$ (Szkody et al. 2003). The time-resolved APO spectra showed the strong modulation and deep transient absorption in the He I and Balmer line cores that characterize SW Sex systems (Szkody et al. 2003). He II and CN emission are present at all phases of the APO spectra.

7. CV accretion disks

Frank, King, & Raine (1992) discuss the theory of accretion disks. They show that the effective temperature of an accretion disk, in hydrostatic equilibrium and timewise invariant, at a distance R from the accretion disk center, is given by the equation

$$T_{\text{eff}}(R) = \left\{ \frac{3GM\dot{M}}{8\pi R^3\sigma} \left[1 - \left(\frac{R_*}{R} \right)^{1/2} \right] \right\}^{1/4}, \quad (1)$$

where M is the mass of the WD, \dot{M} is the mass transfer rate, and R_* is the radius of the WD. G is the gravitation constant and σ is the Stefan-Boltzmann constant. This equation defines the standard model for the radial temperature profile of a CV accretion disk.

The accretion disk is heated by viscous shear. It is now believed that the physical basis for viscosity is the magnetic instability mechanism (Balbus & Hawley 1991). Lack of knowledge of a physical basis for viscosity in the original study of accretion disks led to introduction of the dimensionless parameter α (Shakura & Sunyaev 1973). An alternate viscosity prescription is to use a Reynolds number, typically indicated by the symbol Re . Pringle (1981) discusses both prescriptions and shows that, for CV accretion disks that undergo outbursts to have temporal characteristics roughly equal to observed values, then the α prescription requires values in the range 0.1–1.0, and the Reynolds number prescription should use values in the approximate range 10^2 – 10^3 . Although important advances have been made in specifying the viscosity profile within an accretion disk annulus (Stone & Balbus (1996); Stone et al. (1996); Balbus & Hawley (1997); Balbus (2002)), it still is not possible to calculate a value of α or Re from fundamental physical principles to use in modeling a particular annulus. An important point is that equation (1) has no explicit dependence on the viscosity parameter. We assume that a single value of the viscosity parameter applies to an entire accretion disk.

We model a CV accretion disk as a nested series of cylindrical annuli. The theoretical model by Hubeny (1990, hereafter H90) provides the model for the individual annuli, with additional development in Hubeny & Hubeny (1998) and an earlier investigation in Kříž & Hubeny (1986). Computer implementation of the model is in TLUSTY (v.200) (Hubeny 1988; Hubeny & Lanz 1995). The calculation of annulus synthetic spectra from the TLUSTY models uses program SYNSPEC (v.48) (Hubeny, Stefl & Harmanec 1985; Hubeny 1990). An annulus synthetic line spectrum includes physical line-broadening effects, such as natural, van der Waals, Stark, or from turbulence. We adopted solar composition for all synthetic spectra. A useful option in SYNSPEC is to calculate continuum spectra, but also including H and He lines, rather than line spectra.

H90 develops the theory of the vertical structure of an annulus. The vertically-averaged viscosity and its specific value as a function of reference level within the annulus appear explicitly in this theory. The annulus T_{eff} as a function of radial distance from the geometric center is given by equation (1).

Calculation of a model for a single annulus proceeds in four steps: (1) calculation of

a gray model using mean opacities rather than frequency-dependent ones; (2) iteration, starting with the gray model but now using frequency-dependent opacities, while imposing local thermodynamic equilibrium (LTE) excitation relations, until changes in a state vector, at all levels, become less than a prescribed small value, producing a converged model in LTE; (3) relaxing the LTE requirement and iterating to produce a non-LTE model for the continuum; (4) using the model from (3) and including line opacities and again iterating to produce a final non-LTE model.

Our experience is that models for inner annuli typically converge but convergence becomes more and more fragile for larger radius annuli until only a gray model can be calculated. Depending on the mass transfer rate, even the gray model calculations may fail for the largest radius annuli. Based on extensive tests, we find that plots of annulus synthetic spectra progress smoothly from smaller to larger annulus radii, even though the models transition from LTE to gray models. Consequently, to minimize the required amount of computer time, we have used gray models exclusively in this investigation.

7.1. Calculation of synthetic spectra for a CV system

The BINSYN software suite (Linnell & Hubeny 1996) is used to calculate synthetic spectra for comparison with the observational data. For an accretion disk system, BINSYN produces separate output synthetic spectra for the total system, the mass gainer, the mass loser, the accretion disk face, and the accretion disk rim (including a hot spot, if specified). Line-broadening and line displacement due to the Doppler effect are calculated in BINSYN as the programs generate synthetic spectra for the total system and the individual system components. The calculated synthetic spectra require prior assembly of arrays of source synthetic spectra produced externally to BINSYN, one array for each object (mass gainer, accretion disk face, etc.). Thus, for a model corresponding to Table 2 (see below) and with a 3500K secondary star, BINSYN would require 21 synthetic spectra corresponding to the annulus radii in Table 2, a synthetic spectrum for the WD, a synthetic spectrum (in this case duplicating the outer annulus spectrum) for the accretion disk rim, and a synthetic spectrum for the secondary star. For the latter object, since its contribution in the present case is negligible, a single synthetic spectrum meets the formal requirement. Otherwise, because the secondary star fills its Roche lobe, a range of synthetic spectra would be required covering the photospheric variation in T_{eff} and $\log g$. The BINSYN model for the distorted secondary star includes effects of gravity darkening and irradiation by the primary and the accretion disk. Shadowing of the secondary, by the accretion disk, from irradiation by the primary is included.

The number of annuli specified, e.g., in Table 2, must be large enough that interpolation to a non-tabular T_{eff} value can be accurate. The output spectrum is produced by interpolation within the array of synthetic spectra to produce, in effect, a local photospheric model atmosphere at each photospheric segment. Integration over the segments, with proper allowance for Doppler shifts and sources of line broadening, and with suppression of contributions from segments hidden from the observer, then produces the synthetic spectrum for the object (star, accretion disk, rim) at the particular orbital inclination and longitude under consideration. The system synthetic spectrum is the sum of contributions from the separate objects. Stellar objects are represented by the Roche model, including allowance for rotational distortion up to critical rotation.

The accretion disk is represented within BINSYN by a specified number (typically 32) of concentric annuli with fixed radial width but of increasing thickness (see Linnell & Hubeny (1996)), up to a specified rim height. Each annulus is divided into azimuthal segments (typically 90). Note that the number of annuli specified within BINSYN usually exceeds the number of calculated annulus models. This feature is necessary to provide adequate resolution in calculating, e.g., eclipse effects. BINSYN calculates a T_{eff} value for each internally specified annulus (the 32 mentioned above); these are standard model (Frank, King, & Raine 1992) values by default, but an option permits assigning an individual T_{eff} to each annulus. This feature allows evaluation of an arbitrary temperature profile for the accretion disk, including an isothermal model. The program optionally permits calculation of irradiative heating of the accretion disk by the WD, based on a bolometric albedo formalism. The output spectra from BINSYN are in the same mode as the annulus, etc., spectra—either line spectra or continuum spectra (i.e., if the synthetic spectra for the annuli are continuum spectra, that mode having been chosen for the SYNSPEC calculations, then the system, etc., synthetic spectra produced by BINSTN also will be continuum spectra).

BINSYN requires input specification of the inner and outer radii of the accretion disk. This feature provides important flexibility to truncate the disk at an inner radius and to set the outer radius at the tidal cutoff radius as dictated by the mass ratio of the stellar components. The accretion disk temperature profile typically will place all of the accretion disk on the “hot branch” required for dwarf novae outbursts by the Disk Instability Model, hereafter DIM (Osaki 1996).

8. WD and secondary star masses and T_{eff} values

The observed spectra of SDSSJ0809 give no immediate indications of an underlying WD spectrum, apparently preventing a direct determination of the WD T_{eff} . The sub-

sequent discussion shows that SDSSJ0809 has an accretion disk, so it is clear that the secondary star must fill its Roche lobe. Recent years have seen major progress in models of low-mass stars (Baraffe et al. 1995, 1997, 1998) and recent papers (Kolb & Baraffe 2000; Andronov & Pinsonneault 2004) detail the application of these models to the secondary stars in CVs. From Figures 2 and 3 of Kolb & Baraffe (2000) we determine a secondary component spectral type of about M3 and a secondary component mass $M_2/M_\odot = 0.30 \pm 0.10$. This determination has used the theoretical ZAMS, and there is a substantial difference between observationally determined spectral types and the theoretical ZAMS in the period range 2–5^h. This difference leads to the large uncertainty in the secondary component mass. Subsequent sections consider the propagation of this uncertainty into the system geometry.

Smith & Dhillon (1998) specify an average WD mass of $0.69M_\odot$ for WDs below the period gap and $0.80M_\odot$ for WDs above the period gap. Their tabulation includes only one object in the period interval 2^h to 4^h, and it is a polar. The systems with periods between 4^h and 5^h have WD masses between $0.6M_\odot$ and $1.26M_\odot$, with unreliable values in several cases. The 192 min period places the system above the period gap. For the purposes of an initial illustration we adopt a WD mass of $1.0M_\odot$, and with an uncertainty of $0.2M_\odot$.

The lack of deep eclipses sets an upper limit on the orbital inclination. The presence of absorption cores associated with emission features (Figure 3), (Szkody et al. 2003), with the absorption cores going below the continuum level, sets a rough lower limit on the inclination. We have determined the orbital inclination for which the secondary component barely fails to eclipse the accretion disk rim, both for the $q = 0.30$ case and for a $q = 0.20$ case. For the $q = 0.30$ case, the inclination is $i = 65^\circ$, and for the $q = 0.20$ case the inclination is $i = 67^\circ$. We take the observed low-amplitude light curve, together with the absorption cores in spectral lines, as evidence of a grazing eclipse of the accretion disk by the secondary star and adopt an orbital inclination of $i = 65^\circ$.

Figure 5 shows theoretical radial velocity curves for both cases. The solid curves are the radial velocity curves for the $q = 0.30$ case; the smaller amplitude curve represents the WD while the larger amplitude curve is the secondary star. The dashed curve represents the WD for the $q = 0.20$ case, with $i = 67^\circ$. Gamma velocities of -105 km sec^{-1} and 8 km sec^{-1} were subtracted from $H\alpha$ and $H\beta$, respectively. These velocities were determined empirically by minimizing the sum of the residuals from the theoretical radial velocity curve. The curves show the insensitivity of the system to the value of q . We stress that this paper does *not* argue that the $H\alpha$ and $H\beta$ radial velocities track the WD motion in SW Sex systems in general and in this system in particular.

Figure 6 shows a projection view of the $q = 0.30$ system. A plot for the $q = 0.20$ case is closely similar to Figure 6.

Panei, Althaus, & Benvenuto (2000) determine a radius of $r_{\text{wd}} = 0.00771 R_{\odot}$ for a WD mass of $1.00 M_{\odot}$ and a homogeneous Hamada-Salpeter carbon model. For a secondary star mass of $0.30 M_{\odot}$, and assuming the secondary is similar to a main sequence star of the same mass, we adopt a polar T_{eff} of 3500K for the secondary star (Baraffe et al. 1998). The following analysis will show that the secondary star makes a negligible contribution to the system shortward of 7000Å.

Several SW Sex stars have high WD T_{eff} values. Examples include DW UMa, 40,000K–50,000K (Knigge et al. 2000; Araujo-Betancor et al. 2003; Hoard et al. 2003), and UUAqr, 34,000K (Baptista, Steiner, & Cielinski 1994). Similarly, MV Lyr, a well-known novalike CV, has a T_{eff} of 47,000K (Hoard et al. 2004). We chose a test T_{eff} of 35,000K for SDSSJ0809, with the possibility in mind of a subsequent revision upward (or downward).

9. Initial estimate of mass transfer rate and the accretion disk tidal cutoff radius

The spectroscopic similarity of SDSSJ0809 to an SW Sex system also suggests our initial choice of mass transfer rate. SW Sex stars (for reviews see Hellier (2000); Groot, Rutten & van Paradijs (2000); Hoard et al. (2003)) are novalike (NL) objects with mass transfer rates above the critical rate to avoid disk outbursts (Osaki 1996). From Osaki (1996), the critical mass transfer rate is $\dot{M}_{\text{crit}} \cong 4.28 \times 10^{-9} (P_{\text{orb}}/4^{\text{hr}}) M_{\odot} \text{yr}^{-1}$. In the case of SDSSJ0809, the Osaki expression gives a critical rate of $3.4 \times 10^{-9} M_{\odot} \text{yr}^{-1}$, but we expect there may be appreciable case-to-case variation. Patterson (1984) predicts a mass transfer rate of $2.5 \times 10^{-10} M_{\odot} \text{yr}^{-1}$ at the top of the period gap, while Hameury et al. (1988) determine a value of $1.0 \times 10^{-9} M_{\odot} \text{yr}^{-1}$. We discuss annulus models for four mass transfer rates in the following sections.

A number of studies have considered the tidal cutoff boundary, r_{d} , of accretion disks (Paczynski (1977); Papaloizou & Pringle (1977); Whitehurst (1988); Schwarzenberg-Czerny & Różyczka (1988); Whitehurst & King (1991); Goodman (1993); Warner (1995)). Equation 2.61 in Warner (1995), gives a tidal cutoff radius of $0.49D$, where D is the separation of the stellar components. The other authors cited agree on $r_{\text{d}} \cong 0.33D$. The latter prescription gives a tidal cutoff radius of $51r_{\text{wd}}$, where r_{wd} is the WD radius. In this connection, the difference in D between a $q = 0.30$ system and a $q = 0.20$ system is relatively small. Consequently, the cutoff radius of the accretion disk is insensitive to q .

CVs whose mass transfer rates are above the critical rate, and so are stable, are expected to have an accretion disk temperature profile given by the standard model (Frank, King, & Raine 1992). Smak (1982) finds that the critical temperature for instability in the DIM model

(Lasota 2001) occurs at $T_{\text{eff}} \cong 6300\text{K}$. The standard model with the $r_d = 0.49D$ cutoff radius produces outer annuli T_{eff} values which are below the critical temperature for instability. The $r_d = 0.33D$ cutoff radius produces an outermost annulus T_{eff} value that is at or above the critical temperature for a mass transfer rate of at least $1.0 \times 10^{-9} M_{\odot} \text{yr}^{-1}$. This result agrees with the study by Smak (1983), that NL systems have outer radii whose T_{eff} values lie above the critical temperature. (We thank J.-P. Lasota for a communication on this point.) We adopt the tidal cutoff radius $r_d = 0.33D$ for this system, and note that the WD mass and system mass ratio are uncertain, with a corresponding uncertainty in the exact cutoff radius.

10. Annulus models for four mass transfer rates

Without independent information on the mass transfer rate, we used rates typical for systems with periods between 3-4 hrs. To this end we have calculated standard models for a range of mass transfer rates characteristic of SW Sex stars and have found the best-fitting model for each mass transfer rate. We calculated four sets of accretion disk annuli with the adopted WD mass of $M = 1.0 M_{\odot}$. We chose mass transfer rates of $\dot{M} = 1.0 \times 10^{-9} M_{\odot} \text{yr}^{-1}$, $2.0 \times 10^{-9} M_{\odot} \text{yr}^{-1}$, $3.0 \times 10^{-9} M_{\odot} \text{yr}^{-1}$, and $5.0 \times 10^{-9} M_{\odot} \text{yr}^{-1}$. Table 2 lists annulus properties for the mass transfer rate we ultimately chose as most likely.

The TLUSTY default value for viscosity is $\alpha = 0.1$, and since this is the value widely used for the “hot branch” in the DIM, we adopt it (Pringle 1981; Smak 2000; Tout 2000; Lasota 2001). The viscosity prescription strongly affects the annulus vertical structure, including the annulus optical thickness (Kříž & Hubeny 1986; Hubeny 1990). The TLUSTY parameters ζ_0 and ζ_1 control the vertical viscosity profile in an annulus. We have used the default values which assure that there is no “thermal catastrophe” (Hubeny 1990; Hubeny & Hubeny 1998). The “thermal catastrophe” results when the vertical viscosity profile requires appreciable energy dissipation in low density layers where cooling from strong resonance lines of light metals becomes important.

The TLUSTY models all produce a standard model T_{eff} (Frank, King, & Raine 1992) for an individual annulus. The standard model requires all of the thermal energy generated within an annulus to result from viscous dissipation. Our current models also include irradiation of the disk by the WD, which can modify the standard model $T_{\text{eff}}(R)$ relation.

The chemical composition of the inner annuli, extending to a transition radius described below, include H and He as explicit atoms, and the remaining first 30 atomic species as implicit atoms. Inclusion as an implicit atom means that the atomic species contributes

to the total number of particles and the total charge, but not to the opacity. The vertical temperature profile of a given small radius annulus varies smoothly from the central plane to the upper boundary of the annulus. At larger radii the temperature profiles show increasingly steep drops toward the upper boundary. For these annuli we “switched on” convection in TLUSTY. In addition, the larger radius annuli have lower T_{eff} values, and opacity due to metals is included. Beginning at $T_{\text{eff}} \approx 12000\text{K}$, our annulus synthetic spectra include H, He, C, Mg, Al, Si, and Fe as explicit atoms and the remaining first 30 atomic species as implicit atoms. Because they have fairly high-lying first excited states, N and O do not contribute importantly to the continuum opacity of interest (photoionization from the ground state is close to the Lyman limit, indeed shortward of it for O).

The data for a given annulus have been extracted from an extensive TLUSTY tabulation of physical properties at all (typically 70) reference levels in the annulus, from the central plane to the upper boundary. Note from the last column of Table 2 that all annuli are optically thick. This condition, that all annuli are optically thick, is also true for all of the other mass transfer rates calculated.

The outer annuli for the mass transfer rate of $1.0 \times 10^{-9} M_{\odot} \text{yr}^{-1}$ have outermost annulus T_{eff} values that fall below the stability limit for the DIM model. Smaller mass transfer rates have appreciably larger fractions of the outer annuli that fall below the stability limit. This sets a lower limit on the mass transfer rates to consider.

11. System models for successive mass transfer rates

We began with a standard model $T(R)$ for a mass transfer rate of $1.0 \times 10^{-9} M_{\odot} \text{yr}^{-1}$ and an untruncated accretion disk. Because the *FUSE2* exposure was closer to the time of the *HST* exposure than the *FUSE1* exposure, we initially chose the *FUSE2* spectrum for comparison with our simulations. (The number of plots required to show the results for all four mass transfer rates would be very large. Consequently we present illustrative plots for only one of the mass transfer rates. Similarly, we tabulate annulus properties for only one of the four mass transfer rates (Table 2)). A continuum spectrum fit to the *FUSE2*, *HST* and SDSS spectra for the untruncated disk had far too much UV flux as compared with the *HST* and *FUSE2* spectra. This implied too large a contribution from high T_{eff} annuli. From equation (1), the only way to reduce those contributions, and maintain the standard model, is to truncate the inner accretion disk. Accordingly, we started with the outer radius at the tidal cutoff radius and calculated models truncated at inner radii of 1.0, 4.0, 6.0, 7.5, 8.2, 9.0, and 10.0 times the WD radius. We calculated continuum spectra for the models and determined individual scaling factors to fit them to the SDSS spectrum, requiring

accurate superposition among the models at the long wavelength end of the SDSS spectrum. A model truncated at 8.2 times the WD radius was the best overall fit to the *FUSE2*, *HST*, and SDSS spectra, as judged visually. It would be very difficult to be quantitative in this estimate, since the degree of departure from a good fit in the optical must be weighed against what is an approximate fit to the *HST* and *FUSE* spectra. In addition, the many UV emission line features make location of the continuum problematic. The illustrative plots explain this difficulty. The synthetic spectrum spectral gradient was clearly too shallow in the fit to the SDSS spectrum, and was slightly too hot in the UV. The UV discrepancy increased on substituting the *FUSE1* spectrum. Since the *FUSE1* spectrum provides a more stringent UV constraint on the models (setting a maximum WD contribution), and since the *FUSE1* spectrum mates fairly smoothly with the *HST* spectrum in their overlap region, while the *FUSE2* spectrum does not, we decided to use the *FUSE1* spectrum in our final comparisons between the models and the observed spectra. It is possible that the higher excitation *FUSE2* spectrum results from a higher mass transfer rate from the secondary star.

A slight increase in the truncation radius, to 9.0 times the WD radius, made the fit to the optical spectrum slightly worse without a great improvement in the UV fit. Since the system synthetic spectrum had too much UV flux, and since increasing the truncation radius did not help, we tested the other option of reducing the WD T_{eff} . Substituting a 20,000K WD reduced the WD contribution to the synthetic spectrum to a nearly negligible value, and improved the UV fit.

A mass transfer rate of $2.0 \times 10^{-9} M_{\odot} \text{ yr}^{-1}$ presented the same problem for an untruncated accretion disk. Following the procedure of the previous mass transfer rate, we started with the outer radius at the tidal cutoff radius and calculated models truncated at inner radii of 1.0, 4.0, 6.0, 8.0, 9.7, and 12.0 times the WD radius. The 9.7 model produced a very good fit to the optical (SDSS) spectrum but was too hot in the UV. As with the first mass transfer rate, substituting a 20,000K WD substantially improved the UV fit.

We next considered a mass transfer rate of $3.0 \times 10^{-9} M_{\odot} \text{ yr}^{-1}$. We started with the outer radius at the tidal cutoff radius and calculated models truncated at inner radii of 1.0, 4.0, 8.0, 12.0, 14.3, 16.0, and 18.0 times the WD radius. Figure 7 shows the superposition of these models on the optical spectrum. Note the progression from a too large spectral gradient to a too small gradient for the synthetic spectra. It clearly is possible to select a best fitting model in this spectral region, by visual inspection, from among the available choices. Although we have a χ^2 fitting procedure available, we do not believe its use is warranted in the present illustration. Figure 8 connects the optical region to the UV. Note the large separation of the synthetic spectra in the UV for relatively small differences in the

optical. Figure 9 shows the fits in the UV only. The best overall fit appears to be the model with inner truncation radius $r = 16.0r_{\text{wd}}$. (For brevity, the subsequent text will use “the 16.0 model” to reference this model, and similarly for other inner truncation radii.) The 14.3 model is too bright in the 1100Å to 1350Å interval while the 18.0 model has a large flux discrepancy longward of 1250Å. Figure 10 shows the fit of the 16.0 model to the optical spectrum, and Figure 11 shows the fit to the UV spectra. The Figure 10 result, that the contribution of the secondary star is essentially negligible in the optical, and completely so in the UV, applies to all of the models in this investigation. The fit of the 14.3 model to the optical spectrum is nearly identical to Figure 10. From Figure 7, the 18.0 model (the lowest of the seven plots) has a clearly too small spectral gradient in the optical. This discussion illustrates how we can use visual estimates to select the best fitting model. Plots for other mass transfer rates show characteristics comparable to those shown here but with specific differences described for those mass transfer rates.

For comparison, Figure 12 substitutes the *FUSE*2 spectrum. Note that, in Figure 11, the *FUSE*1 spectrum and the *HST* spectrum fit reasonably smoothly in the overlap region, 1150Å to 1200Å, while there is a clear discontinuity in the Figure 12 overlap. This comparison justifies our use of the *FUSE*1 spectrum. An uncertainty remains for the SDSS spectrum because of its non-simultaneity with the *HST* or *FUSE* spectra.

The fit to the *FUSE*1 spectrum shown in Figure 11 places the synthetic spectrum too high in the vicinity of 1150Å. Figure 13 shows the result of substituting a 20,000K WD. The WD contribution, barely visible at the bottom, now is nearly negligible. The fit near 1150Å is improved but the flux deficit longward of 1300Å is larger.

The same procedure was followed for the mass transfer rate of $5.0 \times 10^{-9} M_{\odot} \text{ yr}^{-1}$. We calculated a set of five models which bracketed the *HST* spectrum from too much to too little flux, with the synthetic spectra normalized to agree with the optical spectrum at 9200Å. All of these models showed a too large spectral gradient on comparison with the optical spectrum. All of the models were too hot in the *FUSE* range, for a 35,000K WD. Substituting a 20,000K WD improved the UV fit but in the *FUSE* range the synthetic spectrum still was too hot. With this substitution, as with the other mass transfer rates, the WD contribution became negligible.

Larger mass transfer rates would produce still greater discrepancies in the fits. Consequently, we do not consider larger mass transfer rates. The best-fitting model at the minimum mass transfer rate, $1.0 \times 10^{-9} M_{\odot} \text{ yr}^{-1}$, is clearly inferior to the best-fitting models at $2.0 \times 10^{-9} M_{\odot} \text{ yr}^{-1}$ and $3.0 \times 10^{-9} M_{\odot} \text{ yr}^{-1}$, which are nearly comparable. The best-fitting model at the maximum mass transfer rate, $5.0 \times 10^{-9} M_{\odot} \text{ yr}^{-1}$, also is inferior to the two intermediate mass transfer rates. We judge that the $3.0 \times 10^{-9} M_{\odot} \text{ yr}^{-1}$ mass transfer rate

is a slightly better spectral fit than the $2.0 \times 10^{-9} M_{\odot} \text{ yr}^{-1}$ rate and adopt the mass transfer rate of $3.0 \times 10^{-9} M_{\odot} \text{ yr}^{-1}$ for this system.

The most important result from the analysis of the four mass transfer rates is that the accretion disk must be truncated if the standard model applies. The fits to the *HST* spectrum exhibit a flux deficiency between about 1400Å and the 1700Å limit of the *HST* spectrum for models that have acceptable flux levels in the *FUSE* range. We see no way to accommodate that discrepancy by maintaining the standard model. If this result is to be accepted, then a physical effect must be introduced to produce the truncation. The two possibilities are evaporation (Menou et al. (2000); Dubus et al. (2001); Lasota (2001)) and interaction with a WD magnetic field. Using the evaporation equation of Menou et al. (2000, eq.3), and setting the evaporation rate equal to the mass transfer rate, it can be shown that evaporation is too small an effect by four orders of magnitude. Groot, Rutten & van Paradijs (2000) state that the SW Sex phenomenon can be explained in the context of a non-magnetic WD, and Rodriguez-Gil et al. (2001) identify circular polarization in the SW Sex star LS Peg, and they argue that magnetic accretion plays a fundamental role in SW Sex stars. Hoard et al. (2003) summarize and describe the various arguments and evidence for and against magnetic WDs in SW Sex stars. Because of this uncertainty, and in anticipation of the results presented in §12, we do not discuss possible truncation of the accretion disk by a magnetic field.

A further important result from the truncation models is that the best fit to the *FUSE* spectrum requires a nearly negligible WD contribution to the system synthetic spectrum. This result is hard to understand, since Figure 6 clearly shows that the inclination is too small for a vertically enlarged accretion disk rim to hide the WD. Hiding the WD would be even more difficult if the accretion disk is truncated. The negligible WD contribution cannot be a result of the accretion disk hiding the WD. The truncation models cover the full range of acceptable mass transfer rates, and a cool WD produces a better synthetic system spectrum fit than the 35,000K WD in all cases. The alternative to hiding the WD behind the accretion disk rim, that the WD actually is cool, is difficult to understand in view of the large mass transfer rate which would be expected to produce a hot WD (Sion 1999; Szkody et al. 2002; Araujo-Betancor et al. 2003). The spreading layer theory applied to WDs (Piro & Bildsten 2004) might permit a prediction of the WD T_{eff} for given M_{WD} and \dot{M} . Although we have found a model which is a fairly good fit to the combined spectroscopic data, the model appears unrealistic and we reject the truncated accretion disk scenario.

We are forced to conclude that the accretion disk in SDSSJ0809 may depart from a standard model, which is the basis of all the models we have calculated to this point.

12. Non-standard model accretion disks

Various studies (e.g., Rutten et al. (1992)), based on image reconstruction, find a flatter temperature profile than the standard $T(R)$ relation. It is of interest to adopt an isothermal accretion disk and test whether that prescription produces a viable model. Figure 14 shows the fits of isothermal 15,500K, 13,000K, and 12,000K untruncated accretion disks to the observed optical spectrum. Figure 15 shows the fits to the *HST* and *FUSE*1 spectra. Each model includes the contribution of a 35,000K WD. The WD contribution, normalized as for the 13000K model, is shown separately at the bottom of Figure 14 and Figure 15. The 12,000K model fits the *HST* spectrum fairly well but has too little flux in the *FUSE* region. All three models are poor fits to the observed optical spectrum.

The tomographic image reconstruction for SW Sex itself (Rutten et al. (1992)) shows that the accretion disk temperature profile follows the standard model in the outer part of the accretion disk, but at a transition radius the temperature profile becomes flat and remains nearly so to the inner edge, with a slow increase. We have implemented a model similar to this reconstruction by first adopting the mass transfer rate, $3.0 \times 10^{-9} M_{\odot} \text{ yr}^{-1}$, for the best standard model, and then finding the radius for which the local T_{eff} was 13,000K. This transition value was based on our result for the isothermal disk models. We used an accretion disk that was not truncated and set the T_{eff} of all annuli within the transition radius equal to 13,000K. The resulting model, in contrast to the isothermal models, fits the optical spectrum very well. However, the fit to the *HST* spectrum left appreciable positive residuals. We experimented with a larger temperature isothermal region, with a smaller radius for the crossover to the standard model. Eventually we found that an isothermal region of 14,000K, with a crossover to the standard model at $r/r_{\text{wd}} = 18.0$, gave a fair representation of the *HST* and *FUSE*1 spectra. (Note that the tidal cutoff radius is at $r/r_{\text{wd}} = 51.3$). The temperature profile of the accretion disk is in Table 5. This model assumes the accretion disk extends to the WD equator, so only half of the WD is visible. The BINSYN software allows for eclipse of inner annuli segments that the WD eclipses.

The fit to the *HST* and *FUSE*1 spectra suggest the possibility of an improved fit with a higher T_{eff} WD. We calculated models, in addition to the 35,000K model, of 40,000K, 45,000K, and 50,000K. All four models have nearly identical fits to the upper (discovery) SDSS spectrum, as shown in Figure 16. The lower (archival) SDSS spectrum is discussed in the following section. Figure 17 shows the fits to the *HST* and *FUSE*1 spectra. The bottom spectrum is the contribution of the accretion disk. Based on the fit near 900Å, the 45,000K model roughly bisects the observed continuum.

The synthetic spectra are given in Eddington flux units; a divisor, s_N , is applied to superpose a synthetic spectrum on the observed spectra. Since the observed flux is tabulated

in units of $1.0 \times 10^{-14} \text{ erg s}^{-1} \text{ cm}^{-2} \text{ \AA}^{-1}$, the distance, d , is given by $d^2 = s_N / 1.0 \times 10^{-14}$. In the present case, for the model using the discovery SDSS spectrum, the scaling factor is 6.1×10^{28} ; the formal derived distance to SDSSJ0809 is 800pc. Note that there is a large associated uncertainty. Tentative system parameters are listed in Table 3. The Table 3 parameters are consistent with other SW Sex systems.

13. The archival SDSS spectrum and model implications

Figure 16 shows the fit of the Table 5 model to the discovery SDSS spectrum. The lower SDSS spectrum is the archival spectrum. Dividing the discovery spectrum by 1.3 and overplotting produces a close fit to the archival spectrum between 5500Å and 9200Å. The discovery spectrum shows increasing positive residuals shortward of 5500Å, reaching a maximum at 4100Å, and decreasing to coincidence with the archival spectrum at 3800Å.

Before attempting to model the archival SDSS spectrum we seek a likely physical basis for the observed change from the discovery spectrum. An important point is that the change took place in only two days. In §11 we have argued that the accretion disk cannot be approximated by a standard model and that models truncated on the inner edge are unrealistic. In §12 we found that isothermal accretion disks produce poorly-fitting models, but that a model whose temperature profile mimics SW Sex satisfactorily fits the discovery SDSS spectrum as well as the UV data. In §11 we have already suggested that the *FUSE2* spectrum differs from the *FUSE1* spectrum because of a higher mass transfer rate. We believe the two SDSS spectra most likely differ for the same reason.

If the mass transfer rate from the secondary star decreases, a cooling wave will propagate inward from the outer accretion disk rim. The temperature of the outer annuli could fall below the transition temperature from the high state. With this scenario in mind, we started with the Table 5 profile, reduced the outer annuli temperatures and calculated a new system model. Although the flux level was reduced, the system synthetic spectrum had a spectral gradient that was too high compared with the archival spectrum. The scaling factor to superpose the synthetic spectrum on either observed spectrum has to remain fixed, since it connects directly to the system distance. We continued temperature reductions for all annuli, reaching the final temperature profile of Table 6. Note that a complete system model was required at each new accretion disk temperature profile. The final fit to the archival spectrum is in Figure 18. Note that Figure 18 presents fits for the same four values of the WD temperature as in Figure 16. Figure 19 shows the four model fits to the UV spectra. Note the large reduction in the contribution of the accretion disk as shown by the lowest plot.

These fits have unacceptably large residuals from the *HST* spectrum. A basic problem is that we have only a single *HST* spectrum and it is not contemporaneous with any of the other observed spectra. No information is available about whether the *HST* spectrum changes in a time interval of days, and by how much.

The proposed scenario to explain the differences in the two SDSS spectra resembles the widely-accepted explanation of VY Sculptoris star behavior (Livio & Pringle 1994; King & Cannizzo 1998). However, SW Sex objects do not undergo the very large brightness variations of VY Scl systems, so the physical cause of mass transfer variation in SDSSJ0809 is uncertain. A detailed study of the high-state/low-state transition in the VY Scl system V794 Aql (Honeycutt, Cannizzo, & Robertson 1994) provides a useful comparison. The drops in V794 Aql brightness have rates that exceed the two-day drop of 0.3 mag. for SDSSJ0809, so the SDSSJ0809 drop rate is not excessive. The theoretical time-dependent model for V794 Aql shows two-day changes in annulus T_{eff} values as large as 10,000K. Also, successive two-day log T_{eff} profiles across the accretion disk are nearly vertical displacements from each other except near the end of the simulation. Thus, the changes from Table 5 to Table 6 appear to be theoretically acceptable, based on a comparison with V794 Aql. The two cases are not entirely comparable since the SDSSJ0809 starting model (Table 5) is not a standard model.

Although it originally appeared reasonable to calculate a system model fitting the combined spectra then available, we conclude that contemporaneous spectra are essential for reliable models of systems which may show significant day-to-day changes. Note that this conclusion is based on a quantitative comparison with model calculations.

14. Discussion

The *FUSE*1 spectrum fits smoothly with the *HST* spectrum in the overlap region, while the *FUSE*2 spectrum does not fit well. This is inconclusive evidence that SDSSJ0809 was in a lower accretion state at the times of both the *HST* and *FUSE*1 exposures, and that the *FUSE*2 spectrum was obtained during a higher state. Because of this uncertainty, we emphasize again that this study has been an illustration of techniques to simulate accretion disks, with the SDSSJ0809 observational data serving as the vehicle for that illustration.

All of these TLUSTY annulus models are optically thick, including the nonstandard models. The optically-thick annulus spectra with their absorption lines and large Balmer discontinuities are in conflict with all of the observed emission line spectra (*FUSE*, STIS, and SDSS). What do the emission lines tell us and what is the most likely way the model

should be changed to produce the observed emission lines? All of the SDSSJ0809 emission lines are single-peaked, one of the defining characteristics of SW Sex stars. In contrast to the SW Sex result that the emission lines arise exclusively from the accretion stream shock (Groot, Rutten & van Paradijs 2000), Hellier (2000) argues for emission lines produced in a wind. Hellier asserts that a wind provides the most straightforward explanation of single-peaked emission lines, and that in particular the wind component fills in any double-peaked disk emission in the Balmer lines. (Also see Drew & Proga (2000)). Table 4 provides some details concerning the Balmer emission lines in SDSSJ0809. There are no P Cygni profiles among the SDSSJ0809 Balmer lines or He lines. There is only a hint of an absorption component at the blue edge of the C IV 1550Å lines.

The most direct explanation of the SDSSJ0809 emission lines is production in a chromospheric or coronal region overlying the accretion disk. Several mechanisms have been proposed that could produce corone: Meyer & Meyer-Hofmeister (1994) use a coronal siphon; Murray & Lin (1992) depend on sound waves that accelerate to form shocks; Liang & Price (1977) propose general nonthermal processes to transport energy vertically from the accretion disk; Hubeny (1990) depends on the vertical variation of viscosity within an annulus; Cannizzo (2000) applies a thermal evaporative instability (Shaviv & Wehrse 1986).

An extensive literature exists relating to formation of emission lines in CV systems. Williams (1980); Tyllenda (1981) and Cheng & Lin (1989) discuss emission line formation in optically thin outer annuli of accretion disks. Ko et al. (1996) discuss emission line formation as a result of X-ray/EUV illumination of the accretion disk by the central object. Horne & Marsh (1986) and Ferguson (1997) discuss emission line formation in more general cases. The SDSS spectrum does not extend far enough in the UV to determine the last resolvable Balmer line; hence, it is not possible to apply the Inglis-Teller equation to determine the electron density where the continuum is produced. Note from Table 4 that the Balmer decrement is relatively flat. (Compare with case A and case B for planetary nebulae, Table 2 of Aller & Liller (1968), and the result that Balmer decrements for some Be stars approximate those of planetary nebulae (Burbidge & Burbidge (1953) and references therein).) Horne & Marsh (1986) point out that in the case of a flat Balmer decrement the Balmer emission lines are optically thick. The fact that all of the annulus models are optically thick, together with the result that the Balmer emission lines are optically thick, is consistent with an origin of emission lines in a chromosphere or corona, not in optically thin outer annuli. Moreover, emission lines produced in optically thin outer regions of an accretion disk occur in a temperature environment of 6000K–9000K (Cheng & Lin 1989). The high excitation emission lines in SDSSJ0809, particularly in the *FUSE* spectra, require a much higher temperature. A notable feature of the observed optical Balmer emission lines is that they are narrower than the synthetic spectrum absorption lines (e.g., see Figure 10).

The model absorption lines are broadened by Keplerian rotation appropriate to the orbital plane. The narrower emission lines could be an indication they are produced well above the accretion disk face, where the horizontal acceleration due to the WD, and the associated Keplerian speed, is smaller.

Extrapolation of the SDSS spectrum indicates the absence of a Balmer jump. la Dous (1989) points out that this condition implies a much lower vertical temperature gradient in an accretion disk than is true in a stellar atmosphere, and likely associates with energy production in the accretion disk, in contrast to a stellar atmosphere.

We doubt that addition of an emission line slab to any of the models will smoothly fill in the absorption lines and convert the absorption line spectrum to the observed emission line spectrum. Rather, we believe that a modification of the individual annulus models is necessary to convert their spectra to emission line spectra. What are the prospects to do this? Hubeny (1990) provides an analytical model for accretion disk annuli that is the basis of the TLUSTY annulus model calculation. As discussed in §10, TLUSTY includes two parameters, ζ_0 and ζ_1 , that specify the vertical viscosity profile in an annulus, and therefore the rate of energy generation as a function of z value. These parameters have default values that prevent a “thermal catastrophe” (Hubeny 1990; Hubeny & Hubeny 1998). Carefully modified values of these parameters can, in principle, produce emission lines.

The Hubeny (1990) analytical model specifically considers conditions that lead to boundary temperatures higher than the annulus T_{eff} . As discussed by Hubeny (1990), the energy dissipated in low density (coronal) layers can be removed by strong (emission) resonance lines of abundant species, such as H I, Mg II, C II, Al III, Si IV, C IV, N V, O VI, etc. Numerical simulations for actual physical models (Stone et al. 1996) indicate that viscosity increases toward the surface, as required for the proposed TLUSTY models. Tout (2000) discusses our present understanding of viscosity, while Hawley (2001) discusses the present status of magnetohydrodynamic simulations of cylindrical Keplerian disks and their relation to viscosity. The calculation of TLUSTY models with modified values of ζ_0 and ζ_1 is beyond the scope of the present investigation.

We have not accounted for the half of the liberated potential energy associated with the mass transfer stream that is usually assigned to accretion luminosity. Part could be dissipated in the shock where the transfer stream merges with the accretion disk. Although BINSYN has the capability to model a rim bright spot, the light curve provides no indication of a bright spot’s existence. A major part of the energy goes into heating the WD. We assume the remainder is carried away in a wind.

An original motivation for analyzing SDSSJ0809 was the hope that visibility of the

WD could be demonstrated. The primary argument for detection of the WD is the model's approximate representation of the UV continuum shortward of 1200\AA . If more extensive observational data support this model, then SDSSJ0809 is very likely an SW Sex star with a high WD T_{eff} in agreement with T_{eff} values for other SW Sex stars.

The authors thank the anonymous referee for detailed comments; addressing them has greatly improved the presentation. The research described in this paper was carried out, in part, at the Jet Propulsion Laboratory, California Institute of Technology, and was sponsored by the National Aeronautics and Space Administration. P.S., D.W.H., K.S.L., and A.P.L. are grateful for support from NASA *FUSE* grant NAG5-13656, NASA *HST* grants GO-09357.06, GO-09724, and AR-10674, and NSF grant AST 02-05875. BTG was supported by a PPARC Advanced Fellowship.

REFERENCES

- Aller, L. H., & Liller, W. 1968, in *Nebulae and Interstellar Matter*, vol. VIII of *Stars and Stellar Systems*, ed. B. M. Middlehurst & L. H. Aller (Chicago:University of Chicago Press), p.483
- Andronov, N., & Pinsonneault, M. H. 2004, *ApJ*, 614, 326
- Araujo-Betancor, S., et al. 2003, *ApJ*, 583, 437
- Balbus, S. A. 2002, in *The Physics of Cataclysmic Variables and Related Objects*, ASP Conf. Ser. 261, ed. B. T. Gänsicke, K. Beuermann and K. Reinsch (San Francisco:ASP) p. 356
- Balbus, S. A. & Hawley, J. F. 1991, *ApJ*, 376, 214
- Balbus, S. A. & Hawley, J. F. 1997, in *Accretion Phenomena and Related Outflows*, IAU Coll. 163, ASP Conf. Ser.121, ed.D. T. Wickramasinge, G. V. Bicknell, & L. Ferrario (San Francisco:ASP) p.90
- Baptista, R., Steiner, J. E., & Cielinski, D. 1994, *ApJ*, 433, 332
- Baraffe, I., Chabrier, G., Allard, F., & Hauschildt, P. H. 1995, *ApJ*, 446, L35
- Baraffe, I., Chabrier, G., Allard, F., & Hauschildt, P. H. 1997, *A&A*, 327, 1054
- Baraffe, I., Chabrier, G., Allard, F., & Hauschildt, P. H. 1998, *A&A*, 337, 404

- Burbidge, G. R., & Burbidge, E. M. 1953, ApJ, 118, 252
- Cannizzo, J. K. 2000, ApJ, 534, L35
- Cheng, F. H., & Lin, D. N. C. 1989, ApJ, 337, 432
- la Dous, C. 1987, Astroph. & Space Sci., 1987, 130, 337
- la Dous, C. 1989, A&A, 211, 131
- la Dous, C. 1994, SSRV, 67, 1
- Drew, J. E., & Proga, D. 2000, New Astronomy Reviews, 44, 21
- Dubus, G., Hameury, J.-M., & Lasota, J.-P. 2001, A&A, 373, 251
- Feldman, P. D., Sahnou, D. J., Kruk, J. W., Murphy, E. M., & Moos, H. W. 2001, J. Geophys. Res., 106, 8119
- Ferguson, D. H. 1997, ApJ, 486, 987
- Frank, J., King, A., & Raine, D. 1992, Accretion Power in Astrophysics (Cambridge: Univ.Press)
- Froning, C. S., Long, K. S., Drew, J. E., Knigge, C., & Proga, D. 2001, ApJ, 562, 963
- Gänsicke, B. T., Szkody, P., de Martino, D., Beuermann, K., Long, K., Sion, E., Knigge, C., Marsh, T., & Hubeny, I. 2003, ApJ, 594, 443
- Goodman, J. 1993, ApJ, 406, 596
- Groot, P. J., Rutten, R. G. M., & van Paradijs, J. 2000, New Astronomy Reviews, 44, 137
- Hameury, J.-M., King, A. R., Lasota, J.-P., & Ritter, H. 1998, MNRAS, 231, 535
- Hawley, J. F. 2001, ApJ, 554, 534
- Hellier, C. 2000, New Astron. Rev., 44, 131
- Hoard, D. W., Szkody, P., Ishioka, R., Ferrario, L., Gänsicke, B. T., Schmidt, G. D., Kato, T., & Uemura, M. 2002, AJ, 124, 2238
- Hoard, D. W., Szkody, P., Froning, C. S., Long, K. S., & Knigge, C. 2003, AJ, 126, 2473
- Hoard, D. W., Linnell, A. P., Szkody, P., Fried, R. E., Sion, E. M., Hubeny, I., & Wolfe, M. A. 2004, ApJ, 604, 346

- Hoard, D. W., Linnell, A. P., Szkody, P., Sion, E. M. 2005, *AJ*, 130, 214
- Honeycutt, R. K., Schlegel, E. M., & Kaitchuck, R. H. 1986, *ApJ*, 302, 388
- Honeycutt, R. K., Cannizzo, J. K., & Robertson, J. W. 1994, *ApJ*, 425, 835
- Horne, K., & Marsh, T. R. 1986, *MNRAS*, 218, 761
- Hubeny, I. 1988, *Comp. Phys. Comm.*, 52, 103
- Hubeny, I. 1990, *ApJ*, 351, 632
- Hubeny, I., Stefl, S., & Harmanec, P. 1985, *Bull. Astron. Inst. Czechosl.* 36, 214
- Hubeny, I., & Lanz, T. 1995, *ApJ*, 439, 875
- Hubeny, I., & Hubeny, V. 1998, *ApJ*, 505, 558
- King, A. R. & Cannizzo, J. K. 1998, *ApJ*, 499, 348
- Knigge, C., Long, K. S., Hoard, D. W., Szkody, P., & Dhillon, V. S. 2000, *ApJ*, 539, L49
- Ko, Y.-K., Lee, Y. P., Schlegel, E. M., & Kallman, T. R. 1996, *ApJ*, 457, 363
- Kolb, U., & Baraffe, I. 2000, *New Astronomy Reviews*, 44, 99
- Kříž, S. & Hubeny, I. 1986, *Bull. Astron. Inst. Czechosl.*, 37, 129
- Lasota, J.-P. 2001, *New Astronomy Reviews*, 45, 449
- Liang, E. P. T., & Price, R. H. 1977, *ApJ*, 218, 247
- Linnell, A. P. & Hubeny, I. 1996, *ApJ*, 471, 958
- Livio, M. & Pringle, J. E. 1994, *ApJ*, 427, 956
- Long, K. S., Wade, R. A., Blair, W. P., Davidsen, A. F., & Hubeny, I. 1994, *ApJ*, 426, 704
- Mauche, C. W. 1999, *ApJ*, 520, 822
- Menou, K., Hameury, J.-M., Lasota, J.-P., & Narayan, R. 2000, *MNRAS*, 314, 498
- Meyer, F. & Meyer-Hofmeister, E. 1994, *A&A*, 1994, 288, 175
- Murray, S. D. & Lin, D. N. C. 1992, *ApJ*, 384, 177
- Osaki, Y. 1996, *PASP*, 108, 39

- Panei, J. A., Althaus, L. G., & Benvenuto, O. G. 2000, *A&A*, 353, 970
- Paczynski, B. 1977, *ApJ*, 216, 822
- Papaloizou, J., & Pringle, J. E. 1977, *MNRAS*, 181, 441
- Patterson, J. 1984, *ApJS*, 54, 443
- Piro, A. L., & Bildsten, L. 2004, *ApJ*, 610, 977
- Pringle, J. 1981, *Ann. Rev. Astron. Astrophys.* 19, 137
- Rodriguez-Gil, P., Casares, J., Martinez-Pais, I. G., Hakala, P., Steeghs, D. 2001, *ApJ*, 548, L49
- Rutten, R. G. M., van Paradijs, J., & Tinbergen, J. 1992, *A&A*, 260, 213
- Sahnou, D. J. et al. 2000, *Proc. SPIE*, 4013, 334
- Schwarzenberg-Czerny, A. & Różycka, M. 1988, *Acta Astron.*, 38, 189
- Shakura, N. I., & Sunyaev, R. A. 1973, *A&A*, 24, 337
- Shaviv, G., & Wehrse, R. 1986, *A&A*, 159, L5
- Sion, E. M. 1999, *PASP*, 111, 532
- Smak, J. 1982, *Acta Astron.*, 32, 199
- Smak, J. 1983, *ApJ*, 272, 234
- Smak, J. 2000, *New Astron.Rev.*, 44, 171
- Smith, D. A., & Dillon, V. S. 1998, *MNRAS*, 301, 767
- Stone, J. M., & Balbus, S. A. 1996, *ApJ*, 464, 364
- Stone, J. M., Hawley, J. F., Gammie, C. F., & Balbus, S. A. 1996, *ApJ*, 463, 656
- Szkody, P., & Piché, F. 1990, *ApJ*, 361, 235
- Szkody, P., Sion, E. M., Gänsicke, B. T., & Howell, S. B. 2002, in *Physics of Cataclysmic Variables and Related Objects*, ASP Conference Series vol. 261 ed. B. T. Gänsicke, K. Beuermann, & K. Reinsch (San Francisco:ASP), p. 21
- Szkody, P., et al. 2003, *AJ*, 126, 1499

- Szkody, P. et al. 2004, AJ, 128, 1882
- Szkody, P. et al. 2005, AJ, 129, 2386
- Thorstensen, J. R., Ringwald, F. A., Wade, R. A., Schmidt, G. D., & Norsworthy, J. E. 1991, AJ, 102, 272
- Tout, C. A. 2000, New Astr. Rev., 44, 37
- Tylenda, R. 1981, Acta Astron., 31, 127
- Wade, R. A., & Hubeny, I. 1998, ApJ, 509, 350
- Warner, B. 1995, Cataclysmic Variable Stars (Cambridge: Cambridge University Press)
- Whitehurst, R. 1988, MNRAS, 233, 529
- Whitehurst, R., & King, A. 1991, MNRAS, 249, 25
- Williams, R. 1980, ApJ, 235, 939

Table 1. *FUSE* Observation Log

Observation #	Exposure #	Start Time		Total Exposure (s)
		(UT)	(HJD–2450000)	
1	1	28 Mar 2003 11:36:10	2726.985218	1590
	2	28 Mar 2003 13:01:23	2727.044391	2473
	3	28 Mar 2003 14:40:37	2727.113297	2515
	4	28 Mar 2003 16:29:19	2727.188776	1888
2	1	16 Mar 2004 14:44:13	3081.116762	3257
	2	16 Mar 2004 16:44:41	3081.200413	2023
	3	16 Mar 2004 18:31:30	3081.274585	1606
	4	16 Mar 2004 20:09:14	3081.342450	1737
	5	16 Mar 2004 21:53:07	3081.414585	1495
	6	16 Mar 2004 23:02:56	3081.463065	2050
	7	16 Mar 2004 23:36:45	3081.486547	1272
	8	17 Mar 2004 00:43:58	3081.533221	560

Note. — “Total Exposure” will be longer than the final usable exposure time because of data that are rejected for quality reasons during the standard pipeline processing.

Table 2. Properties of accretion disk with mass transfer rate $\dot{M} = 3.0E(-9)M_{\odot}\text{yr}^{-1}$ and WD mass of $1.0M_{\odot}$.

r/r_{wd}	T_{eff}	m_0	T_0	$\log g$	z_0	Ne	τ_{Ross}
1.36	66333	8.967E3	54213	7.16	4.63E7	1.11E15	1.48E4
2.00	59475	1.095E4	48448	6.90	8.01E7	6.75E14	1.76E4
3.00	48093	1.070E4	39159	6.60	1.35E8	4.14E14	2.08E4
4.00	40423	9.959E3	32916	6.38	1.94E8	2.90E14	2.39E4
5.00	35062	9.251E3	28556	6.21	2.55E8	2.24E14	2.71E4
6.00	31106	8.639E3	25342	6.07	3.18E8	1.82E14	3.06E4
7.00	28058	8.115E3	22867	5.95	3.81E8	1.52E14	3.39E4
8.00	25630	7.665E3	20894	5.84	4.47E8	1.31E14	3.77E4
10.00	21986	6.934E3	17395	5.67	5.84E8	1.02E14	4.58E4
12.00	19367	6.365E3	15812	5.53	7.24E8	8.21E13	5.42E4
14.00	17381	5.907E3	14201	5.40	8.68E8	6.74E13	6.25E4
16.00	15816	5.529E3	12933	5.30	1.01E9	5.71E13	7.00E4
18.00	14547	5.210E3	11905	5.20	1.16E9	4.96E13	7.60E4
20.00	13495	4.937E3	11054	5.12	1.31E9	4.36E13	7.98E4
22.00	12606	4.700E3	10333	5.04	1.44E9	3.78E13	8.13E4
24.00	11843	4.492E3	9717	4.97	1.59E9	3.25E13	8.10E4
30.00	10086	3.993E3	8287	4.78	2.02E9	1.49E13	7.52E4
34.00	9213	3.734E3	7572	4.68	2.32E9	6.68E12	7.17E4
40.00	8188	3.420E3	6744	4.61	3.13E9	1.87E12	6.97E4
45.00	7516	3.207E3	6202	4.39	2.68E9	5.27E11	6.69E4
50.00	6961	3.026E3	5759	4.18	2.36E9	1.59E11	7.48E4

Note. — Each line in the table represents a separate annulus. The column headed by m_0 is the column mass above the central plane. The column headed by T_0 is the boundary temperature. Compare with T_{eff} . The $\log g$ values are at an optical depth of 0.9. The z_0 column gives the height of the annulus in cm. The accretion disk radius at the tidal cutoff boundary is 2.75×10^{10} cm. The Ne column is the electron density at the

upper annulus boundary. The τ_{Ross} column is the Rosseland optical depth at the central plane. A viscosity parameter $\alpha = 0.1$ was used for all annuli.

Table 3. SDSSJ0809 Model System Parameters

parameter	value	parameter	value
M_{wd}	$1.00 \pm 0.2 M_{\odot}$	r_{wd}	$0.00771 R_{\odot}$
M_{sec}	$0.30 \pm 0.10 M_{\odot}$	$\log g_{\text{wd}}$	8.35
\dot{M}	$3.0 \pm 1.0 \times 10^{-9} M_{\odot} \text{yr}^{-1}$	$r_s(\text{pole})$	$0.311 R_{\odot}$
P	0.133 days	$r_s(\text{point})$	$0.451 R_{\odot}$
D	$1.1901 R_{\odot}$	$r_s(\text{side})$	$0.324 R_{\odot}$
Ω_{wd}	155.7	$r_s(\text{back})$	$0.363 R_{\odot}$
Ω_s	2.46623	$\log g_s(\text{pole})$	4.95
i	$65 \pm 5^{\circ}$	$\log g_s(\text{point})$	-0.44
$T_{\text{eff,wd}}$	$45,000 \pm 5000 \text{K}$	$\log g_s(\text{side})$	4.88
$T_{\text{eff,s}}(\text{pole})$	3500K(nominal)	$\log g_s(\text{back})$	4.67
A_{wd}	1.0	r_a	$0.39 R_{\odot}$
A_s	0.5	r_b	$0.00771 R_{\odot}$
b_{wd}	0.25	H	$0.0096 R_{\odot}$
b_s	0.08		

Note. — wd refers to the WD; s refers to the secondary star. D is the component separation of centers, Ω is a Roche potential. Temperatures are polar values, A values are bolometric albedos, and b values are gravity-darkening exponents. r_a specifies the outer radius of the accretion disk, set at the tidal cut-off radius, and r_b is the accretion disk inner radius, as determined in the final system model, while H is the semi-height of the accretion disk rim, based on the standard model.

Table 4. Features of SDSSJ0809 Balmer emission lines

Identification	FWHM	EW	decrement
$H\alpha$	21.5	21.6	2.5
$H\beta$	14.0	8.78	1.00
$H\gamma$	13.0	5.98	0.68
$H\delta$	12.0	4.85	0.55
$H\epsilon$	14.0 ^a
$H8$	11.0 ^b
$H9$	6.0	1.00	0.11

^aBlended with He II 3968.43Å

^bBlended with He II 3887.44Å

Table 5. Accretion disk temperature profile for discovery SDSS spectrum

r/r_{wd}	T_{eff}	r/r_{wd}	T_{eff}	r/r_{wd}	T_{eff}
1.0000	14,000	16.3448	14,000	34.6581	9079
1.0225	14,000	18.0096	14,000	36.3230	8776
1.3611	14,000	19.6745	13,644	37.9878	8495
3.0260	14,000	21.3393	12,875	39.6527	8234
4.6908	14,000	23.0042	12,200	41.3175	7992
6.3557	14,000	24.6690	11,164	42.9824	7766
8.0205	14,000	26.3339	11,071	44.6472	7554
9.6854	14,000	27.9987	10,593	46.3121	7355
11.3502	14,000	29.6636	10,162	47.9769	7168
13.0151	14,000	31.3284	9768	49.6418	6992
14.6799	14,000	32.9933	9409	51.3066	6826

Table 6. Accretion disk temperature profile for archival SDSS spectrum

r/r_{wd}	T_{eff}	r/r_{wd}	T_{eff}	r/r_{wd}	T_{eff}
1.0000	11,500	16.3448	10,000	34.6581	9000
1.0225	11,500	18.0096	10,000	36.3230	8500
1.3611	11,500	19.6745	10,000	37.9878	8300
3.0260	11,500	21.3393	10,000	39.6527	8100
4.6908	11,000	23.0042	10,000	41.3175	7800
6.3557	11,000	24.6690	10,000	42.9824	7500
8.0205	11,000	26.3339	10,000	44.6472	7200
9.6854	11,000	27.9987	10,000	46.3121	7000
11.3502	10,500	29.6636	10,000	47.9769	6700
13.0151	10,500	31.3284	9500	49.6418	6500
14.6799	10,500	32.9933	9200	51.3066	6200

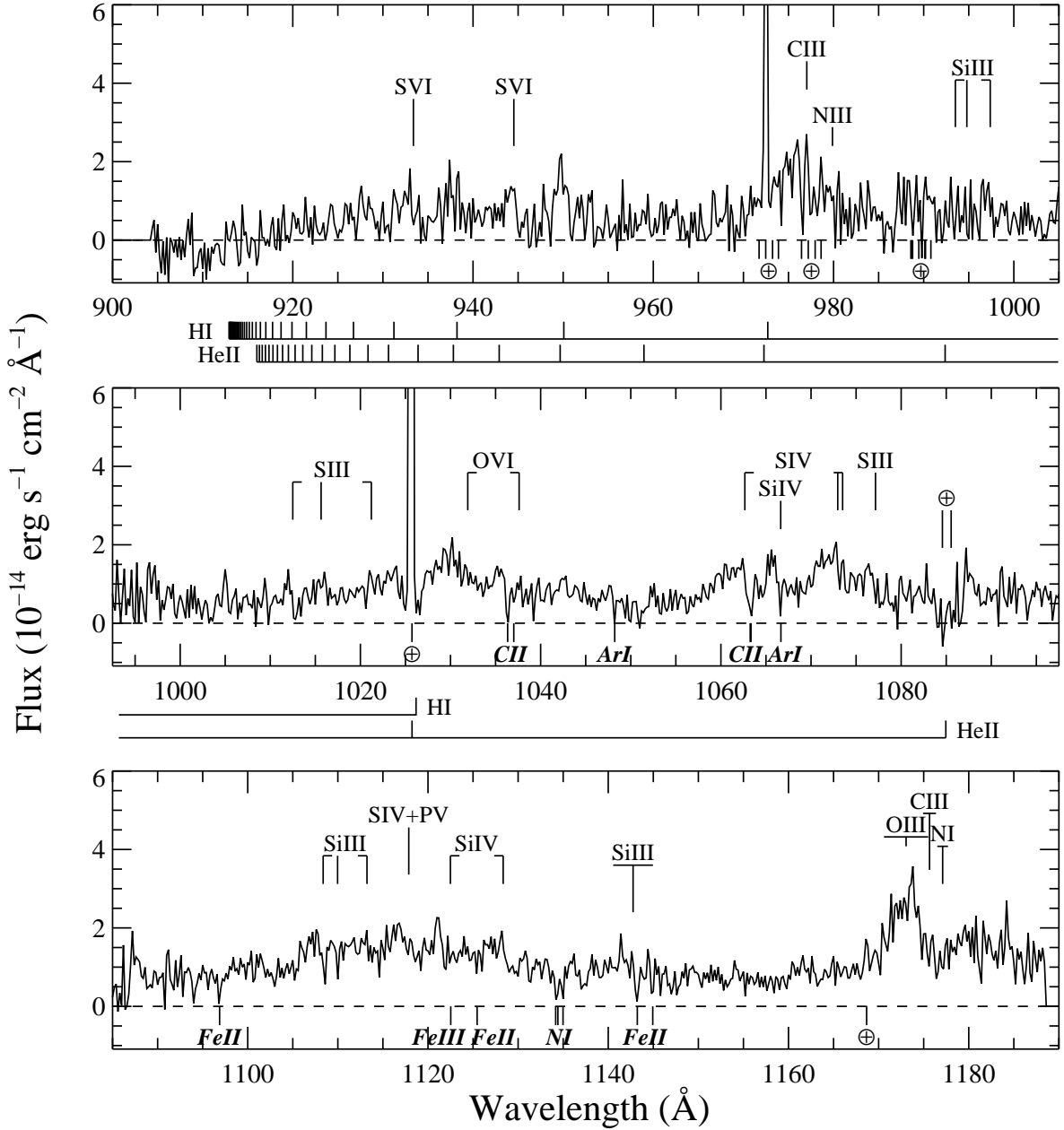


Fig. 1.— Average FUV spectrum of SDSSJ0809 from Observation 1 (2003), binned to a dispersion of $0.20 \text{ Å pixel}^{-1}$. The spectrum spans 915–1185 Å; the top and bottom panels overlap the ends of the middle panel by 7.5 Å. Prominent features often found in FUV spectra of CVs are indicated, although not all of them are present in SDSSJ0809 (see text). Airglow lines (\oplus ; identified from Feldman et al. 2001) and probable ISM lines (ions in *italics*) are indicated below the spectrum. The airglow lines have been truncated at the upper flux limit of the plot. Wavelengths of H I and He II transitions are shown between the panels.

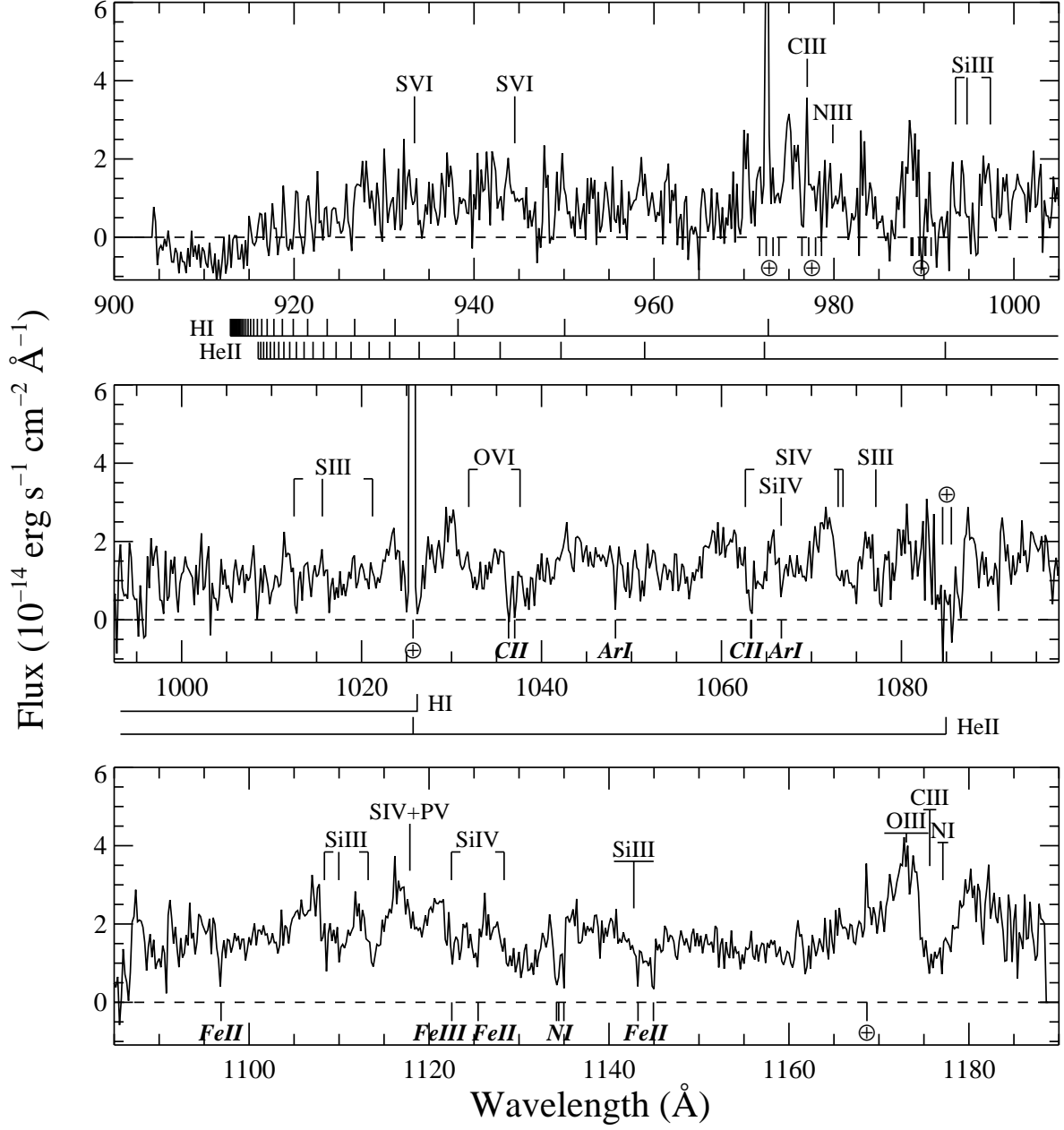


Fig. 2.— As in Figure 1 but showing the average FUV spectrum of SDSSJ0809 from Observation 2 (2004).

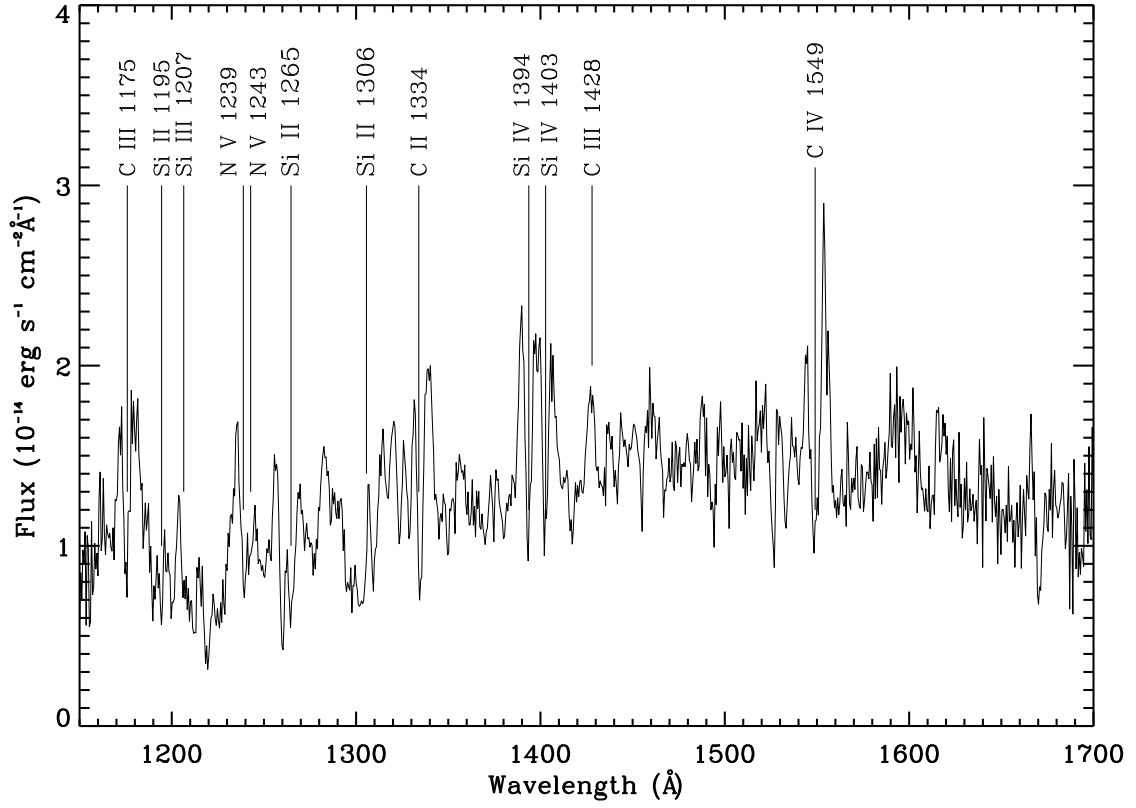


Fig. 3.— *HST* spectrum of SDSSJ0809. Note that several emission features have absorption cores extending below the continuum, indicating a substantial line-of-sight column density.

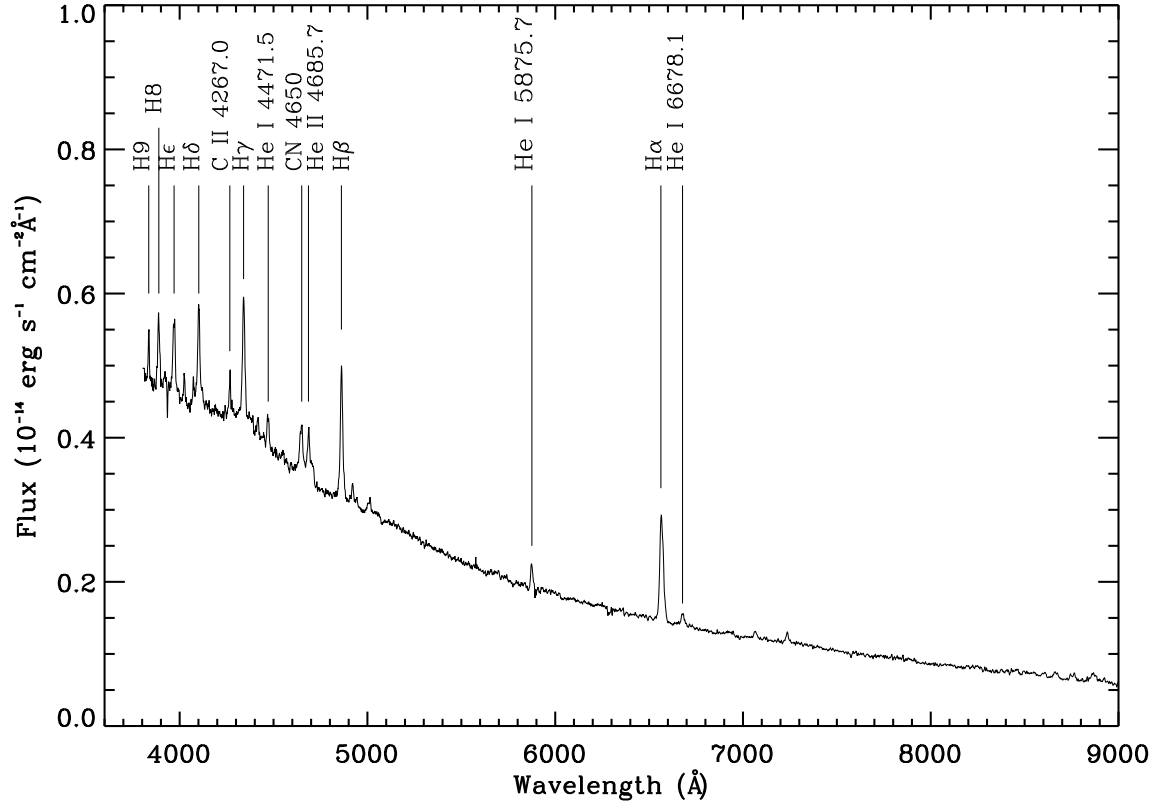


Fig. 4.— Discovery SDSS spectrum of SDSSJ0809. Note the lack of absorption wings on the Balmer lines and the absence of any indication of a Balmer discontinuity.

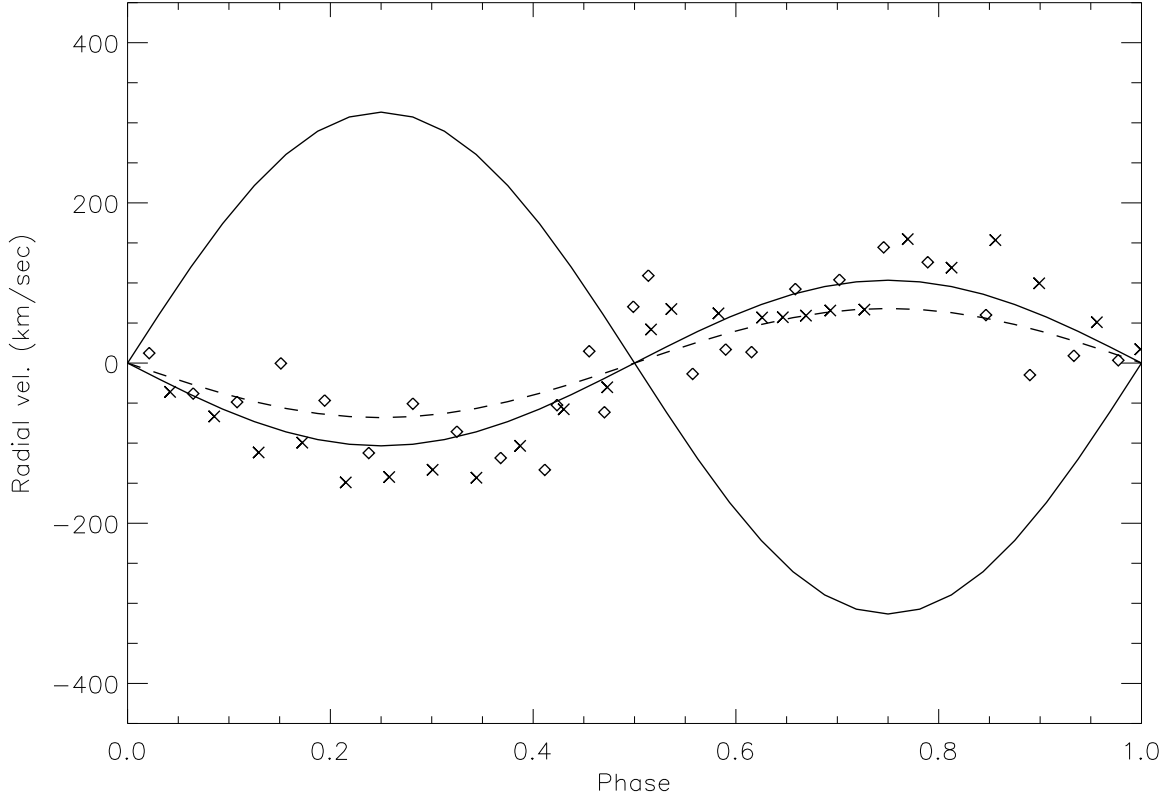


Fig. 5.— Theoretical radial velocity curves of system stars compared with H α (diamonds) and H β (x's) observations. The WD mass is $1.0M_{\odot}$, the mass ratio is $q = 0.30$, the orbital period is 192^{m} , and the orbital inclination is 65° (continuous curves). The dashed curve is the projected WD velocity for a mass ratio of $q = 0.20$.

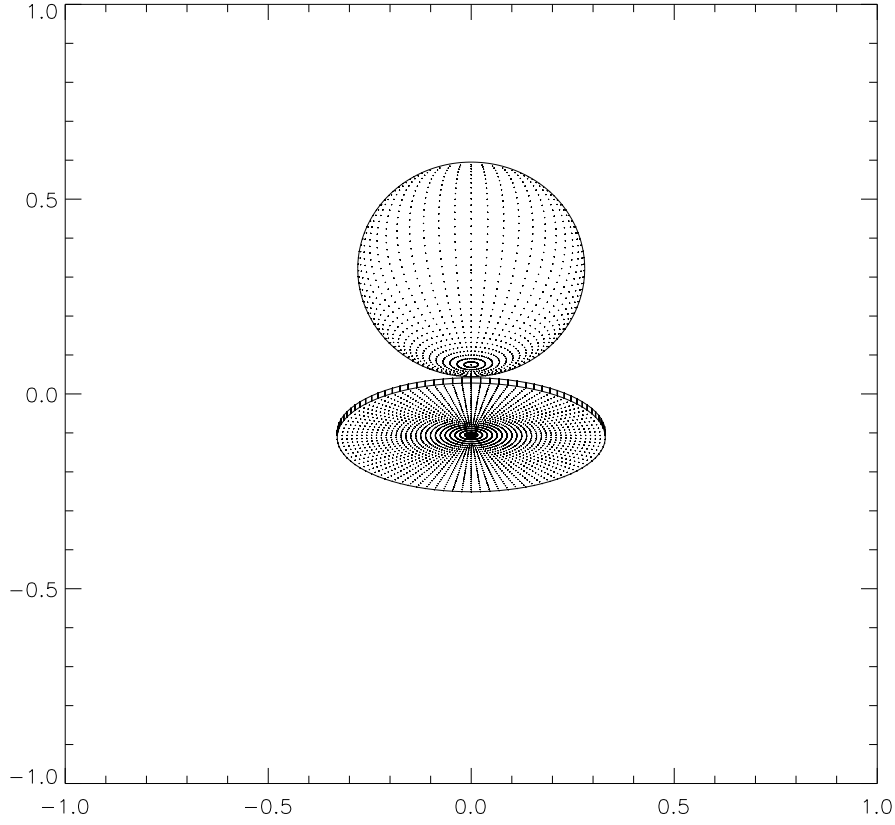


Fig. 6.— View of the system described in Figure 5 at orbital phase 0.0, $q = 0.30$, projected on the plane of the sky for $i = 65^\circ$. This is inferior conjunction for the secondary star; it is between the observer and the WD. The inner edge of the accretion disk extends to the WD equator in this plot (no truncation), and the outer accretion disk radius is at the tidal cutoff radius. The plot for a $q = 0.20$, $i = 67^\circ$ system is closely similar.

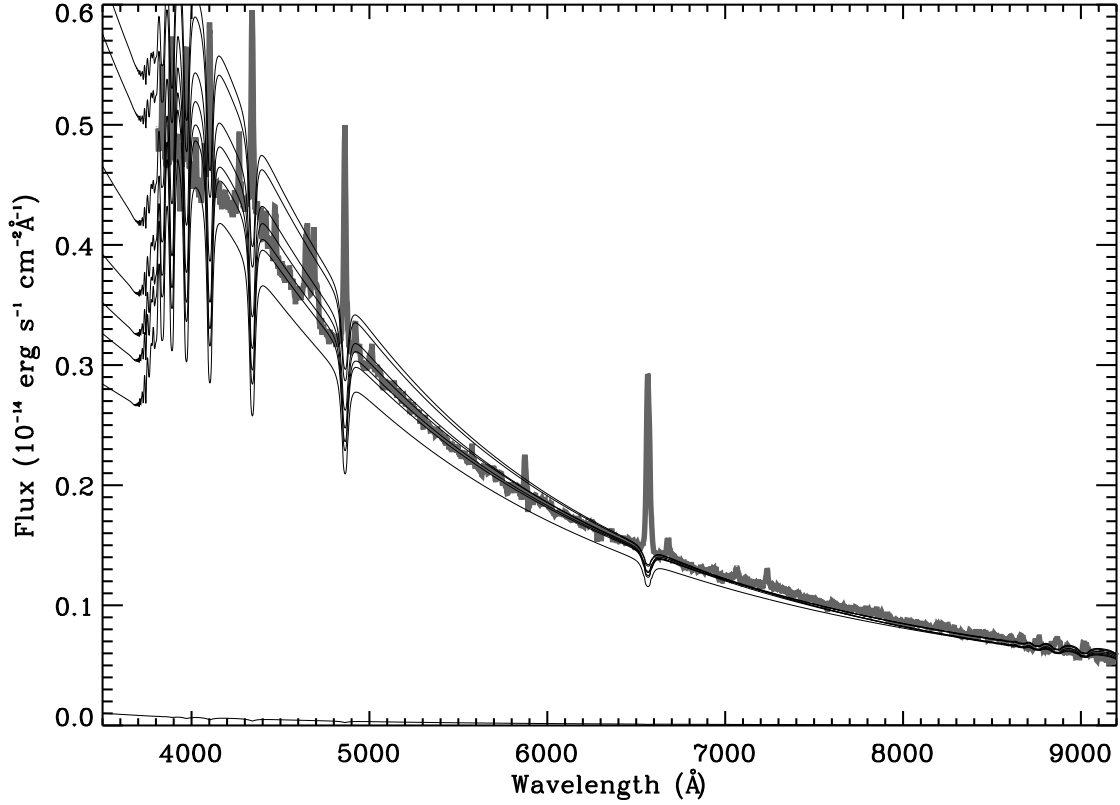


Fig. 7.— Synthetic spectra for truncation radii of (from top to bottom) 1.0, 4.0, 8.0, 12.0, 14.3, 16.0, and 18.0 times the WD radius (thin lines), fitted to the SDSS spectrum (broad line). The mass transfer rate is $3.0 \times 10^{-9} M_{\odot} \text{ yr}^{-1}$. The best fit is the $r = 16.0 r_{WD}$ spectrum; it shows separately in Figure 10.

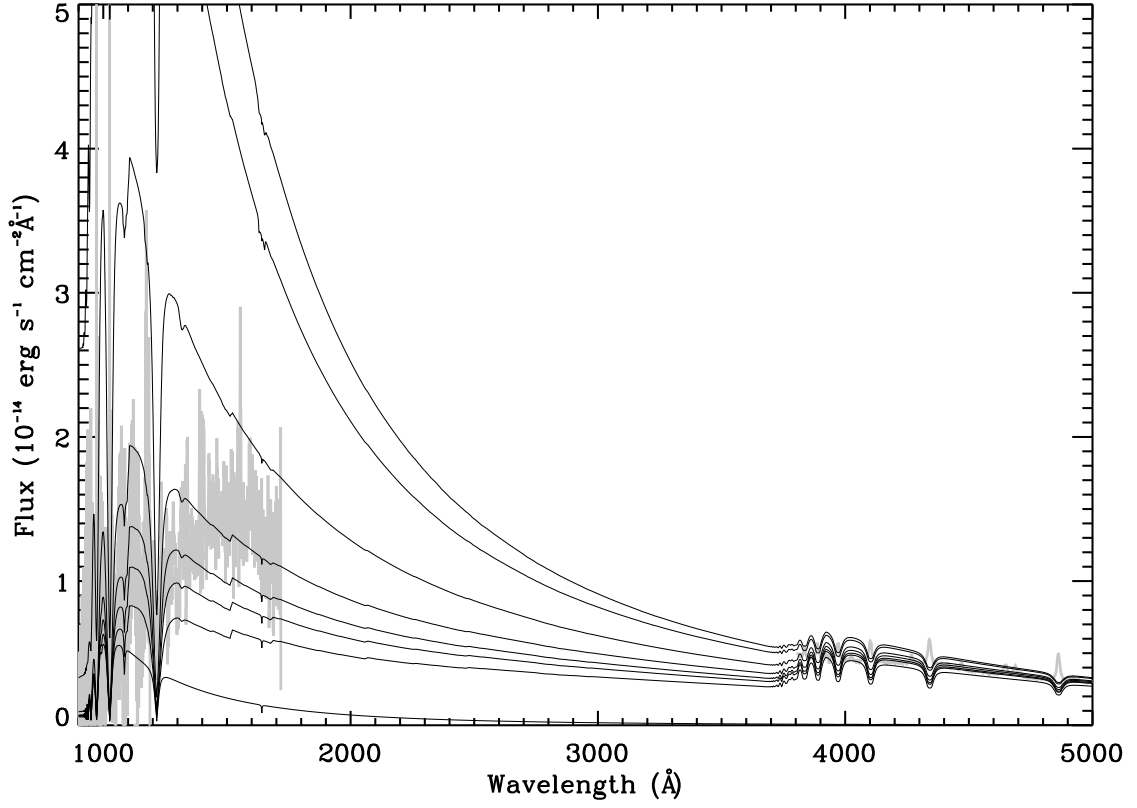


Fig. 8.— As in Figure 7, but extending into the UV region. Note the large separation of synthetic spectra in the UV for a relatively small difference in the optical. The mass transfer rate is $3.0 \times 10^{-9} M_{\odot} \text{ yr}^{-1}$.

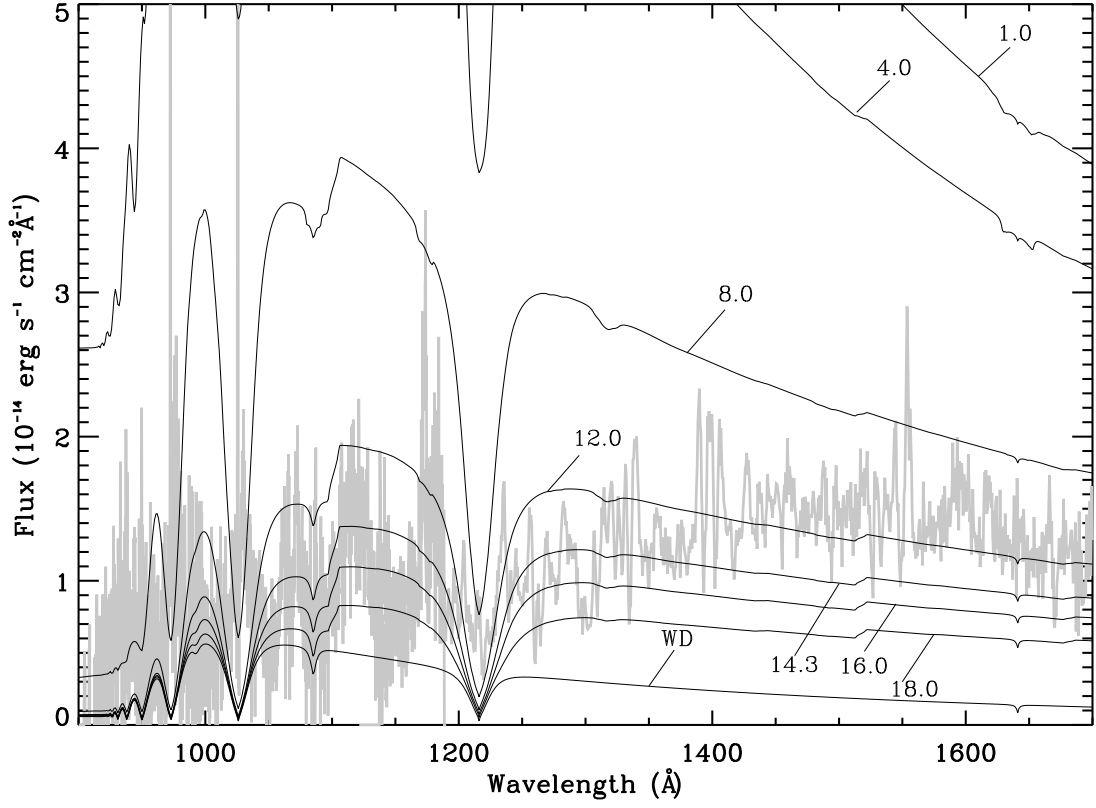


Fig. 9.— As in Figure 8 but showing only the UV. The 35,000K WD model spectrum is at the bottom. The other model spectra are labeled with the disk inner truncation radius (in WD radii).

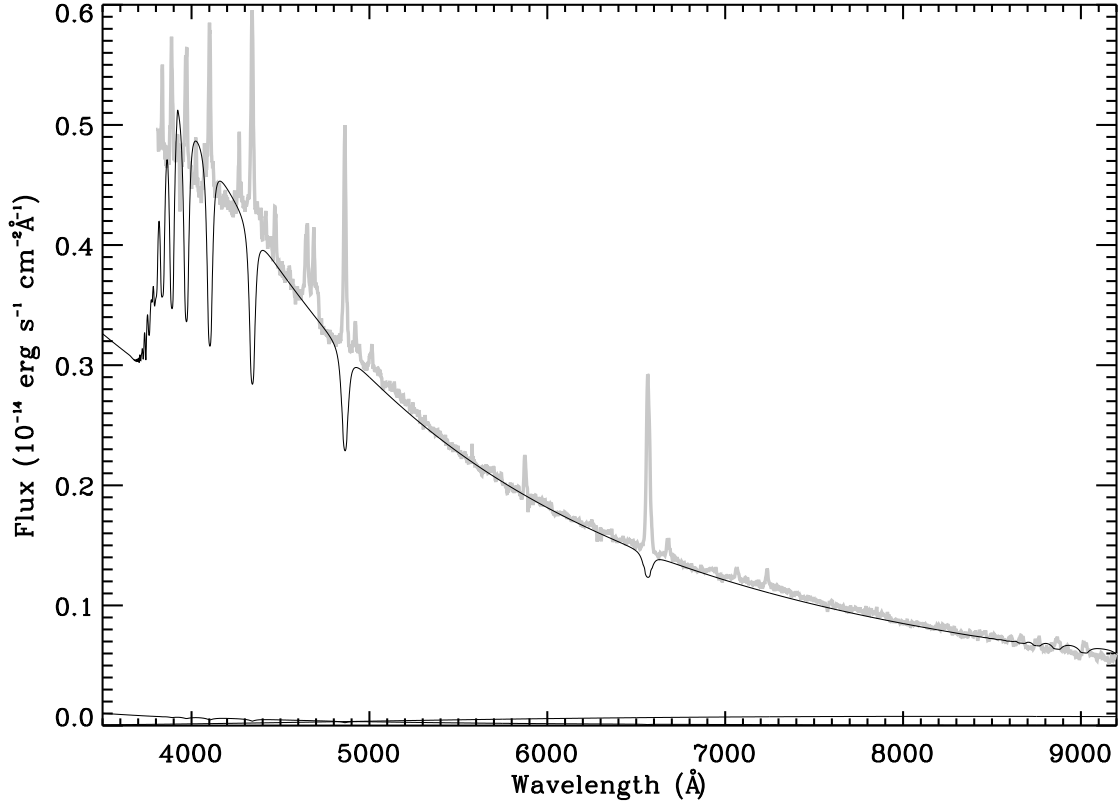


Fig. 10.— Plot showing detail of the $r_{\text{inner}} = 16.0 r_{WD}$ model (dark line) fit to the optical spectrum (light line). The spectrum rising to the bottom right is the secondary star component, and the spectrum rising to the bottom left is the 35,000K WD component.

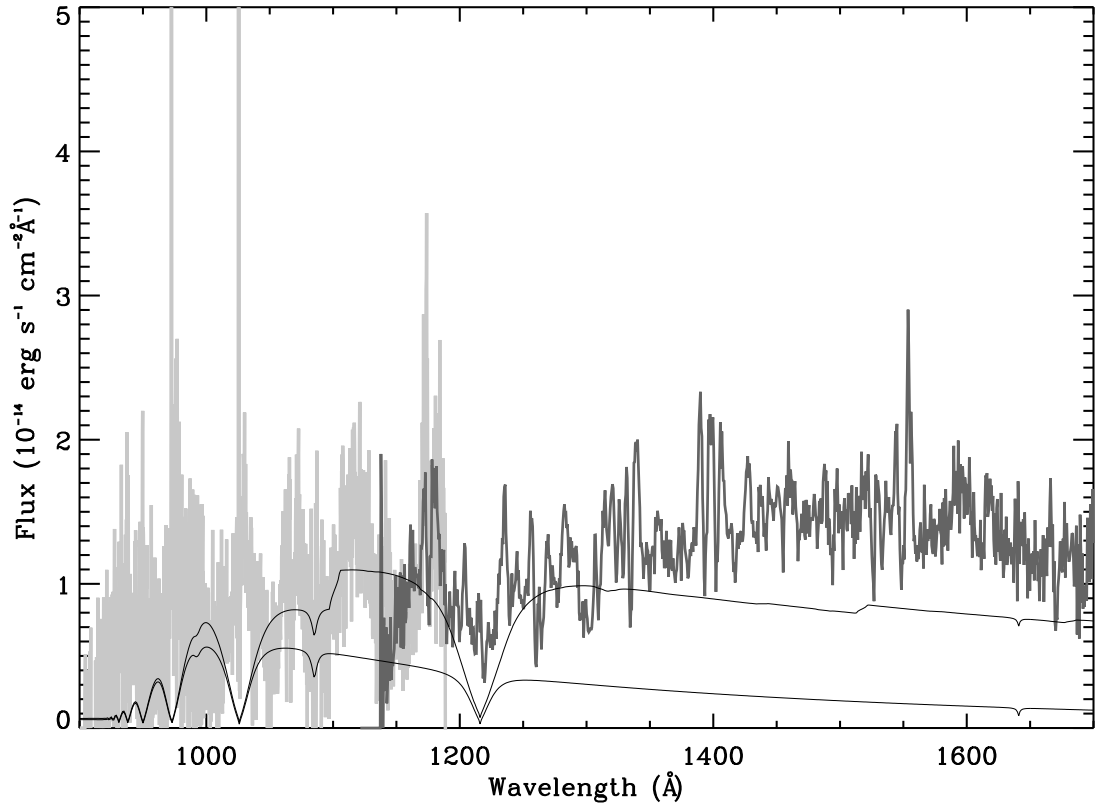


Fig. 11.— As in Figure 10 but for the UV data. Note that the *FUSE1* and *HST* spectra agree well in the overlap region. The 35,000K WD contribution is the lowest spectrum.

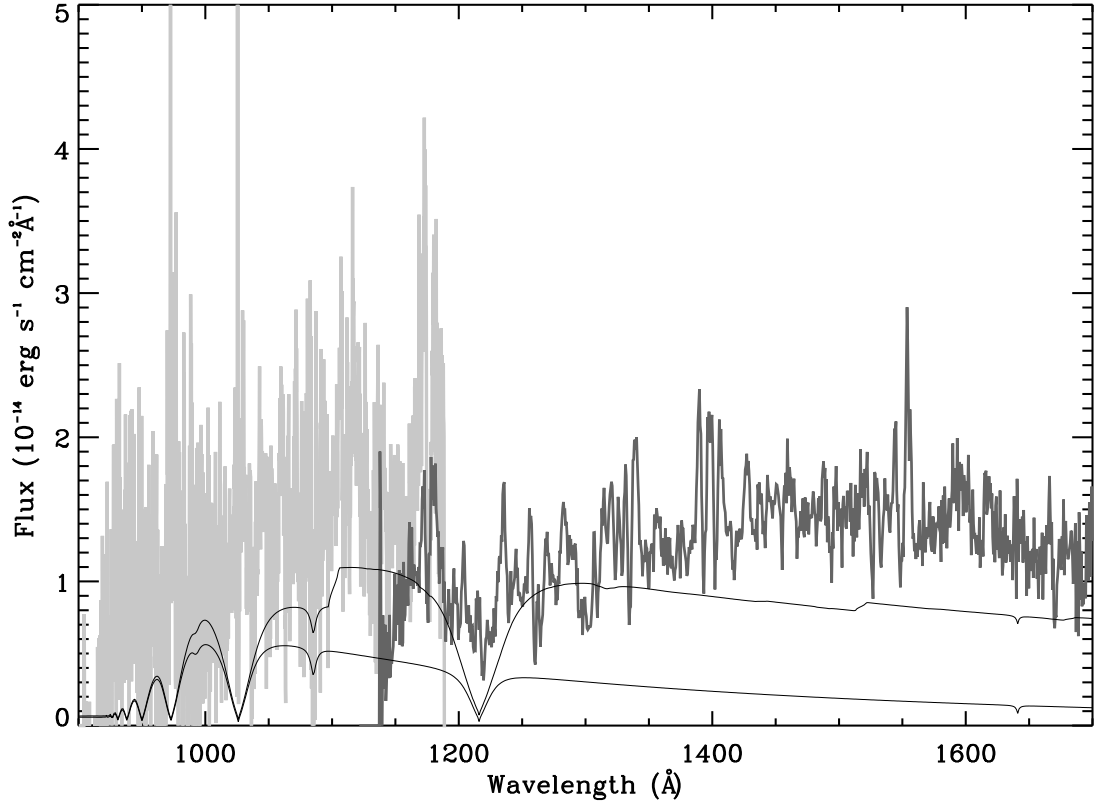


Fig. 12.— As in Figure 11 except the *FUSE2* spectrum has been substituted for the *FUSE1* spectrum. The *HST* and *FUSE2* spectra do not match well in the overlap region. The synthetic spectrum is a poor fit to the *FUSE2* spectrum.

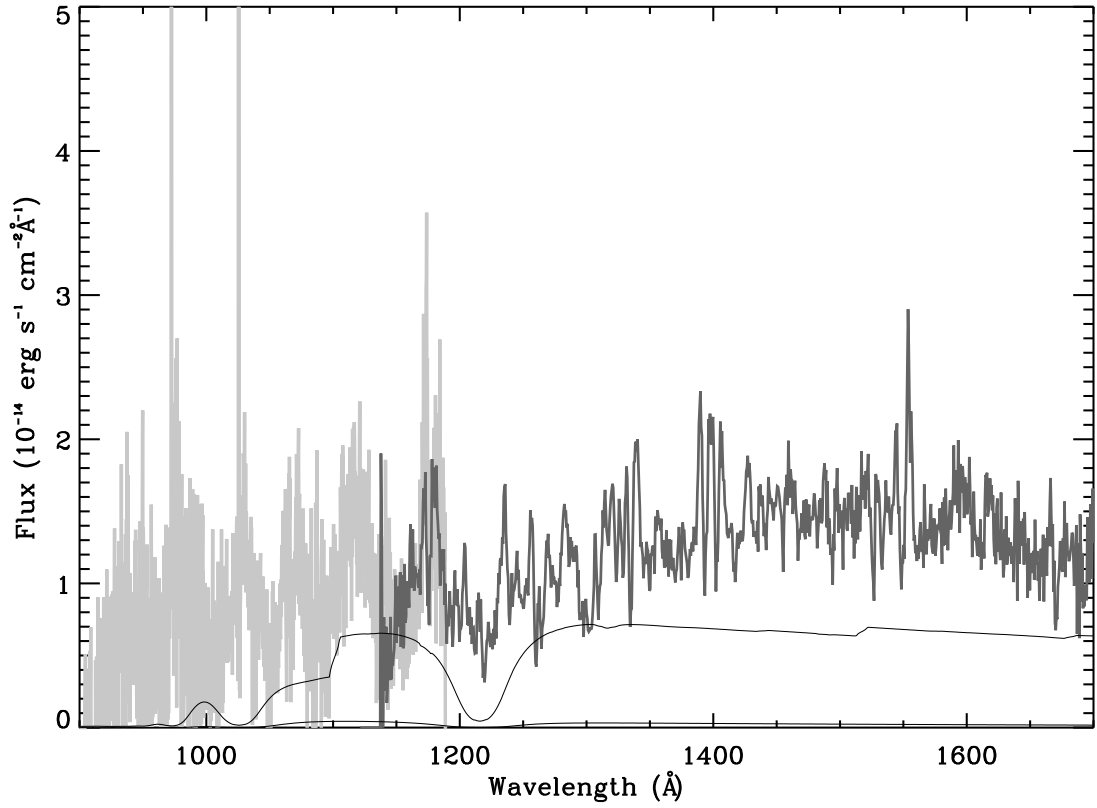


Fig. 13.— As in Figure 11 except a 20,000K WD has been substituted. The synthetic spectrum now passes through the middle of the *FUSE*1 spectrum near 1150Å, but the flux deficit longward of 1300Å is appreciable.

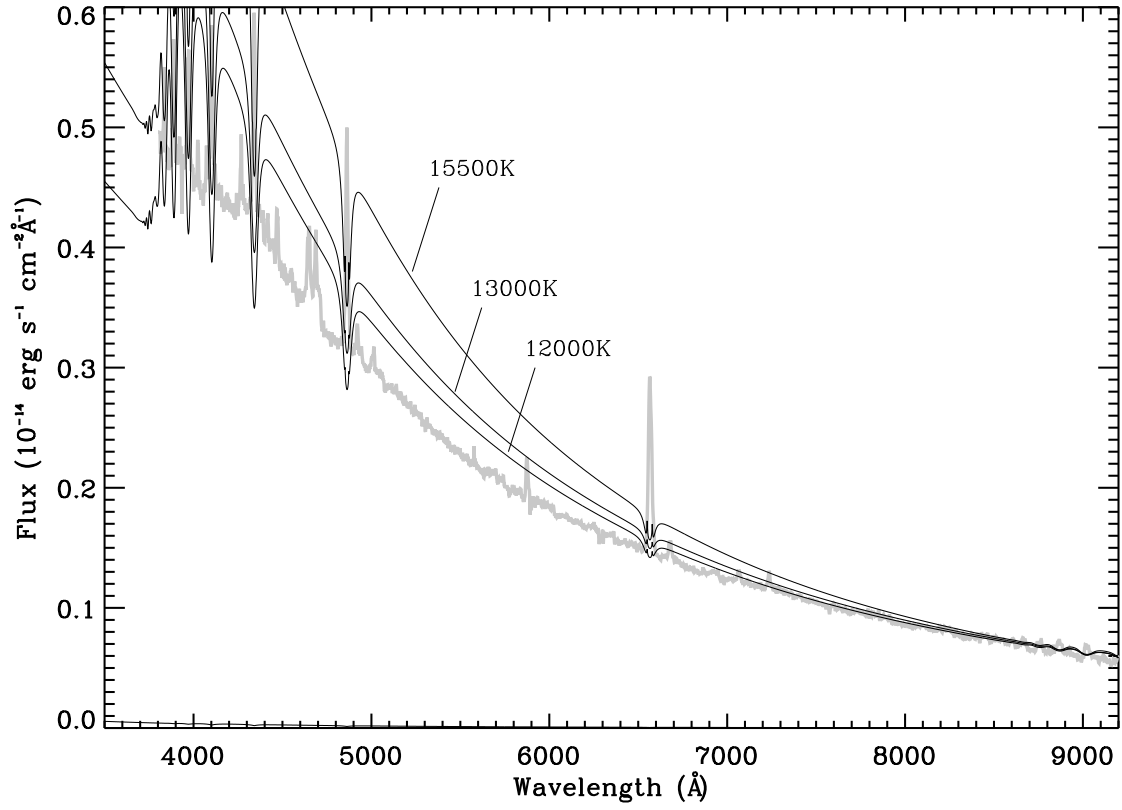


Fig. 14.— Synthetic spectrum for three isothermal accretion disks (untruncated). Note that the spectral gradient is too large in all cases.

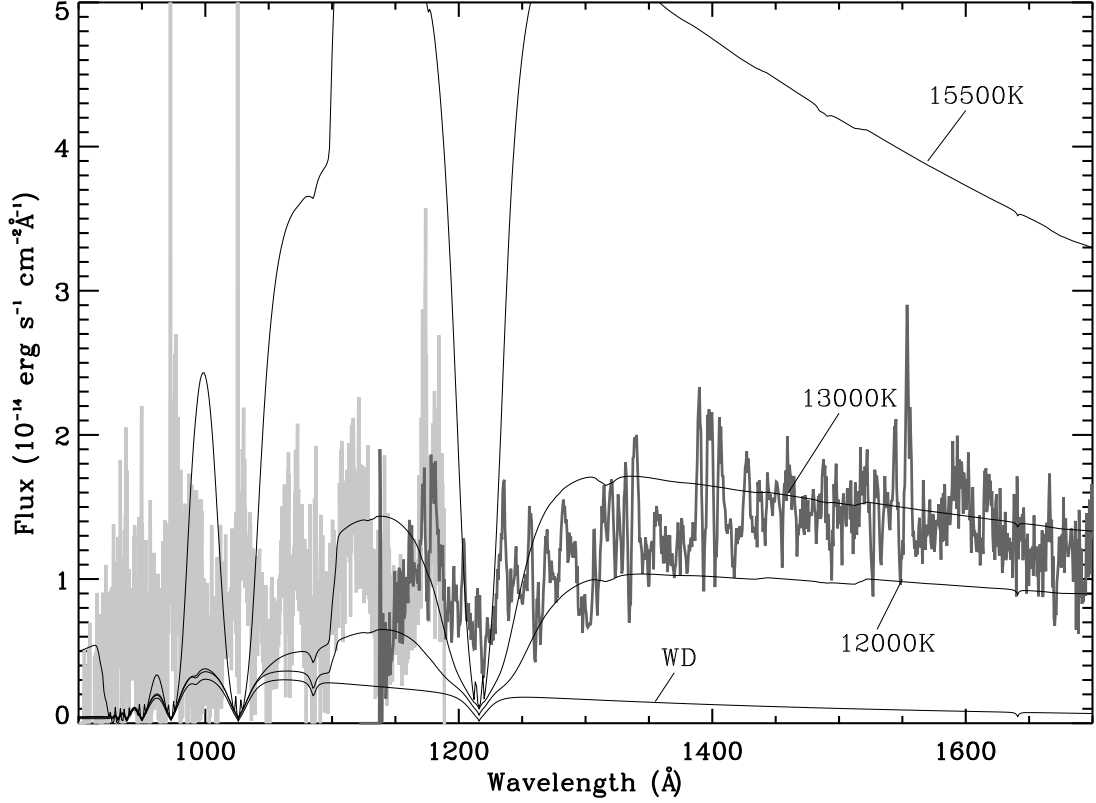


Fig. 15.— As in Figure 9 but showing the isothermal disk models from Figure 14. The relative contribution of the 35,000K WD is less than in Figure 9 because the required scaling factor to superpose the spectra is larger in this case since the accretion disk is not truncated. Note that there is a large discrepancy from the *FUSE*1 spectrum. The 12,000K synthetic spectrum provides the best fit to the *HST* and *FUSE*1 spectra, but the corresponding fit in the optical region is poor.

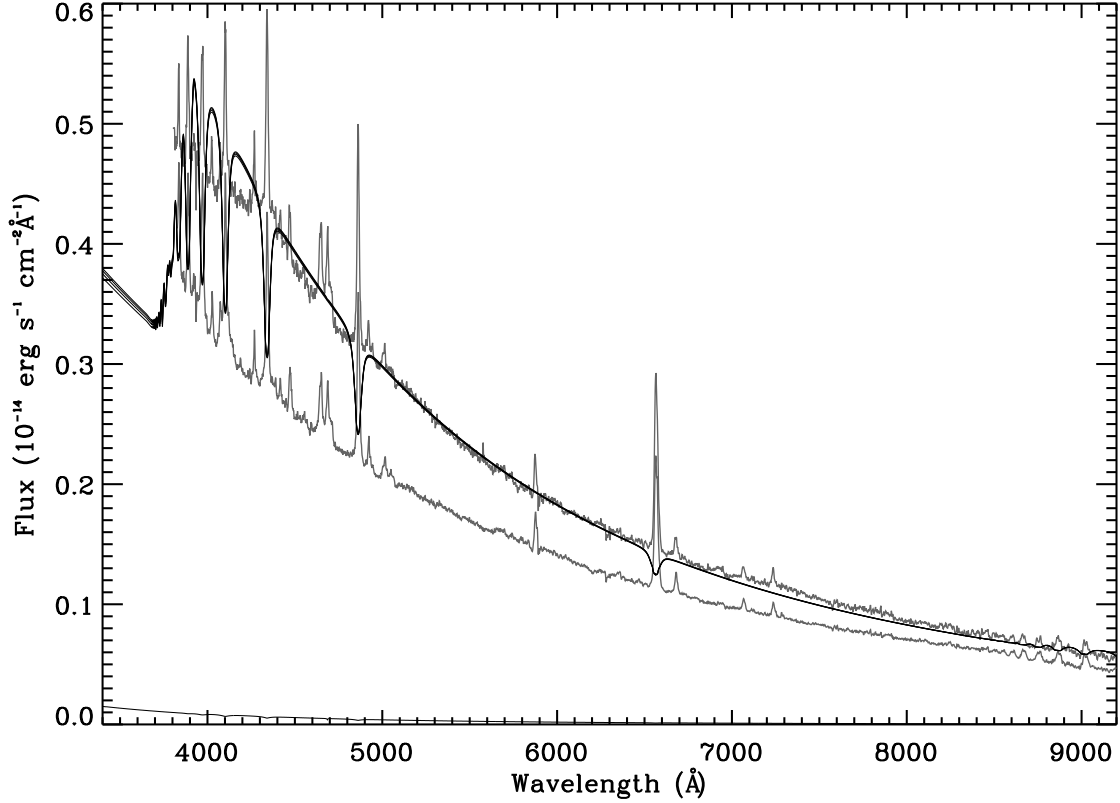


Fig. 16.— Models with four different values of WD T_{eff} and an accretion disk that is isothermal in the inner region and follows a standard model in the outer region. The accretion disk temperature profile is in Table 5. The models fit the discovery SDSSJ0809 spectrum. The other observed spectrum is from the archive. The models are insensitive to the WD T_{eff} at optical wavelengths and are essentially indistinguishable in the figure. The 45,000K WD contribution is at the bottom.

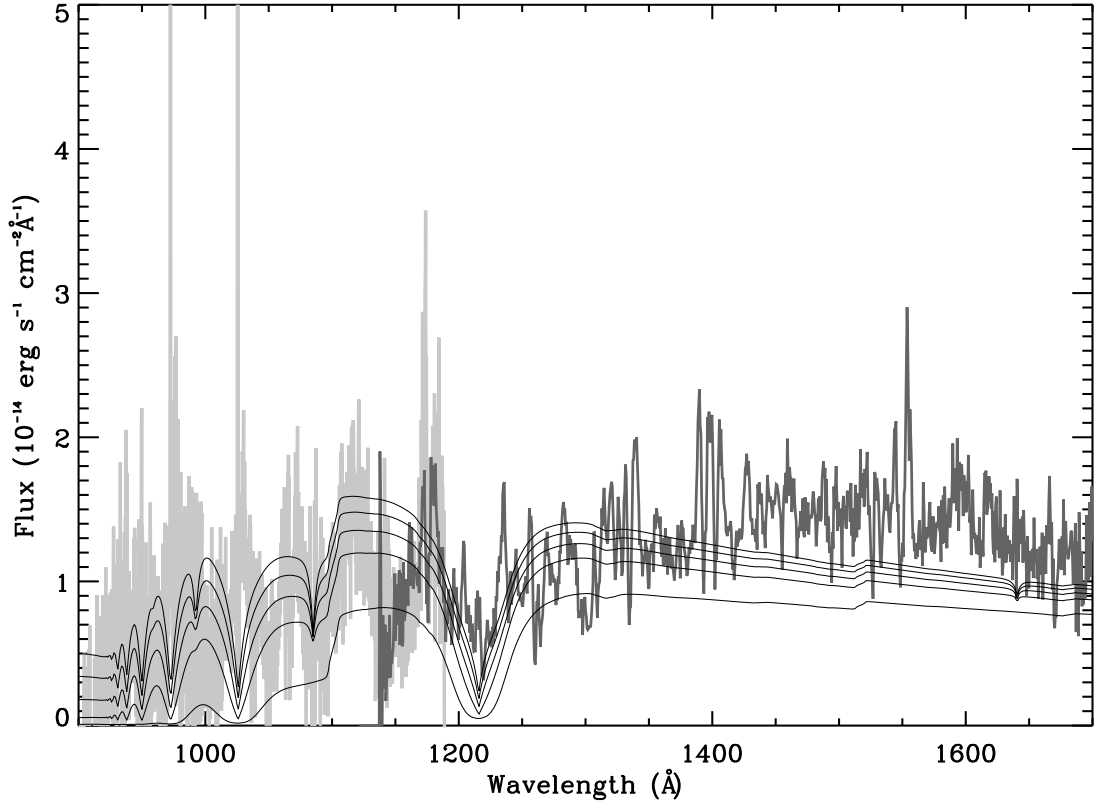


Fig. 17.— As in Figure 16 except in the UV. From top to bottom, the synthetic spectra show the models containing a WD with $T_{\text{eff}} = 50,000\text{K}$, $45,000\text{K}$, $40,000\text{K}$, and $35,000\text{K}$. The lowest synthetic spectrum is the contribution of the accretion disk only.

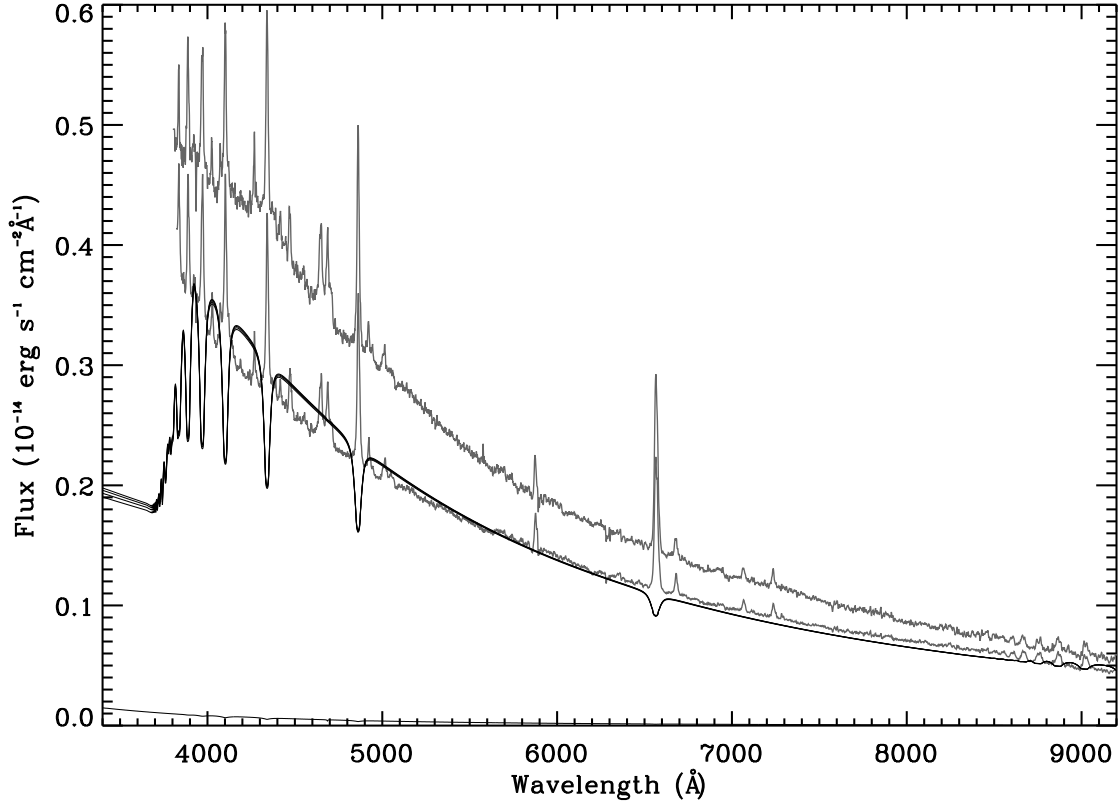


Fig. 18.— Models with four different values of WD T_{eff} and an accretion disk whose temperature profile is in Table 6. The models fit the SDSSJ0809 spectrum from the archive. Compare with Figure 16. The lowest curve is the contribution of a 45,000K WD.

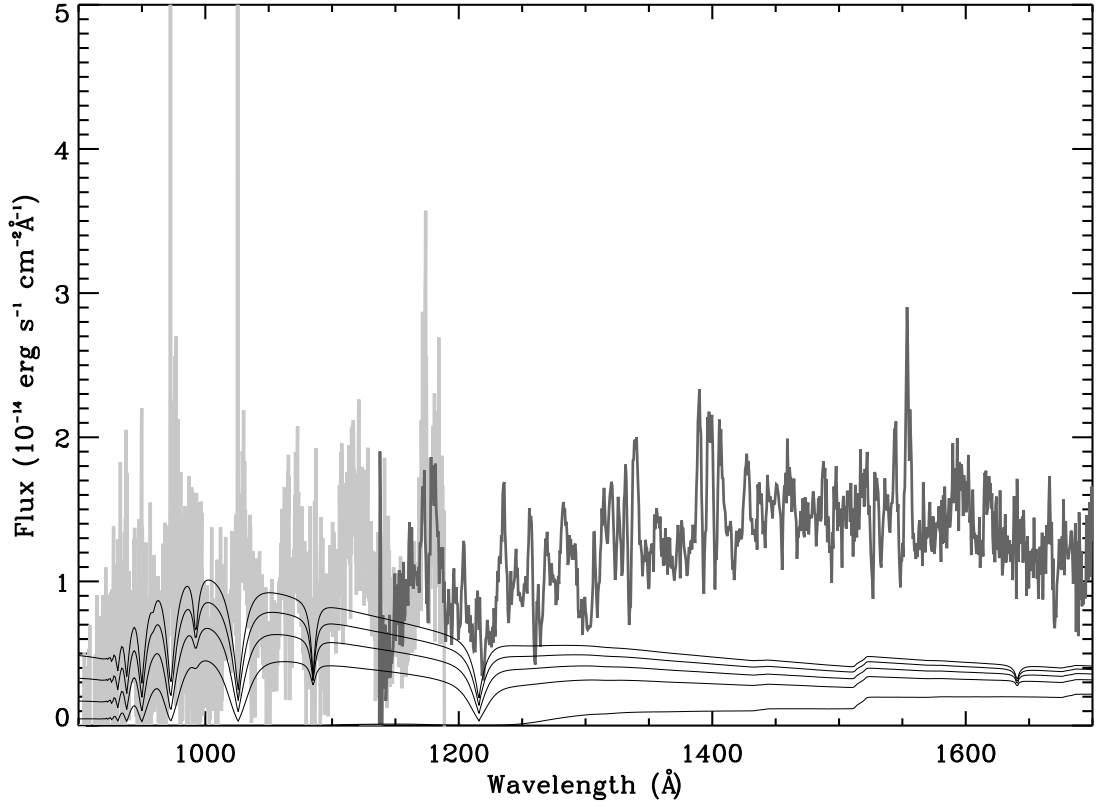


Fig. 19.— As in Figure 18 but showing the UV fit. From top to bottom, the curves are models containing a WD with $T_{\text{eff}} = 50,000\text{K}$, $45,000\text{K}$, $40,000\text{K}$, and $35,000\text{K}$. See the text for a discussion. The lowest synthetic spectrum is the accretion disk contribution only.